

Bimodal morphologies of massive galaxies at the core of a protocluster at $z = 3.09$ and the strong size growth of a brightest cluster galaxy

M. Kubo^{1,2*}, T. Yamada,^{3,4} T. Ichikawa,⁴ M. Kajisawa,⁵ Y. Matsuda,^{6,7}
I. Tanaka,⁸ H. Umehata^{9,10}

¹National Astronomical Observatory of Japan, Osawa 2-21-1, Mitaka, Tokyo 181-8588, Japan

²Institute for Cosmic Ray Research, University of Tokyo, 5-1-5 Kashiwa-no-Ha, Kashiwa City, Chiba 277-8582, Japan

³ISAS/JAXA, 3-1-1 Yunodai, Chuo-ku, Sagami-hara, Kanagawa 252-5210, Japan

⁴Astronomical Institute, Tohoku University, 6-3 Aoba, Aramaki, Aoba-ku, Sendai, Miyagi 980-8578, Japan

⁵Research Centre for Space and Cosmic Evolution, Ehime University, Bunkyo-cho 2-5, Matsuyama 790-8577, Japan

⁶Chile Observatory, National Astronomical Observatory of Japan, Tokyo 181-8588, Japan

⁷SOKENDAI (Graduate University for Advanced Studies), Osawa 2-21-1, Mitaka, Tokyo 181-8588, Japan

⁸Subaru Telescope, National Astronomical Observatory of Japan, 650 North A'ohoku Place, Hilo, HI 96720, USA

⁹Institute of Astronomy, The University of Tokyo, Mitaka, Tokyo 181-0015, Japan

¹⁰The Open University of Japan, 2-11 Wakaba, Mihama-ku, Chiba 261-8586, Japan

in original form 2014 October 31

ABSTRACT

We present the near-infrared high resolution imaging of an extremely dense group of galaxies at the core of the protocluster at $z = 3.09$ in the SSA22 field by using the adaptive optics AO188 and the Infrared Camera and Spectrograph (IRCS) on Subaru Telescope. Wide morphological variety of them suggests their on-going dramatic evolutions. One of the two quiescent galaxies (QGs), the most massive one in the group, is a compact elliptical with an effective radius $r_e = 1.37 \pm 0.75$ kpc. It supports the two-phase formation scenario of giant ellipticals today that a massive compact elliptical is formed at once and evolves in the size and stellar mass by series of mergers. Since this object is a plausible progenitor of a brightest cluster galaxy (BCG) of one of the most massive clusters today, it requires strong size ($\gtrsim 10$) and stellar mass (\sim four times by $z = 0$) growths. Another QG hosts an AGN(s) and is fitted with a model composed from a nuclear component and Sérsic model. It shows spatially extended [OIII] λ 5007 emission line compared to the continuum emission, a plausible evidence of outflows. Massive star forming galaxies (SFGs) in the group are two to three times larger than the field SFGs at similar redshift. Although we obtained the K -band image deeper than the previous one, we found no candidate new members. This implies a physical deficiency of low mass galaxies with stellar mass $M_* \lesssim 4 \times 10^{10} M_\odot$ and/or poor detection completeness of them owing to their diffuse morphologies.

Key words: galaxies: formation — galaxies: evolution — galaxies: distances and redshifts — galaxies: clusters: general

1 INTRODUCTION

There is the well established morphology-density relation in the current Universe where elliptical and S0 galaxies dominate rich cluster cores while spiral galaxies are dominant in general fields (Dressler 1980). The galaxy morphologies are tightly related to properties of galaxies that massive early-

type galaxies (ETGs) are generally dominated by old stars, and with low star formation activities and gas contents. The physical mechanisms that relate morphological transformation and shutting down star formation activity with the environment are still open questions. In mature clusters in the current Universe, harassment (Moore et al. 1996), strangulation (Larson, Tinsley, & Caldwell 1980) and ram-pressure stripping (Gunn & Gott 1972) can play important roles on quenching star formation and transforming morphologies,

* E-mail: mariko.kubo@nao.ac.jp

but on the other hand, red sequences have already appeared in the protoclusters at $z = 2 - 3$ (Kodama et al. 2007; Zirm et al. 2008; Uchimoto et al. 2008, 2012; Kubo et al. 2013), when the galaxy clusters have not yet been fully virialized.

Massive quiescent galaxies (QGs) at up to $z \sim 3$ are now found by deep multi-wavelength surveys in general fields (e.g., Ilbert et al. 2013; Muzzin et al. 2013; Man et al. 2016). Generally, they are remarkably compact compared to massive ETGs today (e.g., Daddi et al. 2005; Trujillo et al. 2006; Toft et al. 2007; van Dokkum et al. 2008; Damjanov et al. 2009; van Dokkum et al. 2010; van der Wel et al. 2014). van Dokkum et al. (2010) and Patel et al. (2013) argue that such compact QGs at $z > 2$ are plausible progenitors of massive ETGs by comparing constant cumulative number density samples of massive galaxies from $z = 0$ to 3. The dissipative processes like gas rich major mergers (Cox et al. 2006; Naab et al. 2007; Wuyts et al. 2010; Bournaud et al. 2011) and/or in-streaming gas by violent disk instabilities (Dekel, Sari, & Ceverino 2009; Ceverino et al. 2015) are proposed as formation scenarios of such compact elliptical galaxies. Series of dry minor mergers can increase the sizes of compact QGs effectively (e.g., Naab, Johansson, & Ostriker 2009). Based on high resolution cosmological numerical simulations, Oser et al. (2010) proposed the two phase formation scenario in which in-situ rapid gas accretion and violent star formation form a compact spheroid at first and it is grown by mergers of galaxies formed at outside of its virial radius.

One of the major uncertainties in the previous studies is the traceability of progenitors of massive ETGs. Protoclusters are suitable targets to study progenitors of galaxies dominating rich cluster cores today. The strong size growths of massive ETGs is supported from many studies of QGs in the protoclusters at $z < 2$ (Zirm, Toft, & Tanaka 2012; Cooper et al. 2012; Papovich et al. 2012; Lotz et al. 2013; Newman et al. 2014; Andreon, Dong, & Raichoor 2016). But it is not still unclear how their evolutions relate to environments at earlier time. To challenge this question, we need to study protoclusters at the epoch when the morphology-density relation just arises.

The SSA22 protocluster at $z = 3.09$ is a rare density peak of galaxies found from the overdensity of Lyman break galaxies (LBGs; Steidel et al. 1998) at first and in later well characterized as a core high density region of a superstructure by the wide field (1.38 deg^2 in the SSA22) narrow-band surveys of Ly α emitters (LAEs) at $z \approx 3.09$ (Hayashino et al. 2004; Yamada et al. 2012). The velocity dispersion of the protocluster core is $\sim 700 \text{ km s}^{-1}$ and the cluster mass measured by using the velocity dispersion or overdensity are $\sim 2 - 5 \times 10^{14} M_{\odot}$ (Kubo et al. 2015). Thus this protocluster is a plausible progenitor of a core of one of the most massive clusters today. In Kubo et al. (2013), we reported that there is an overdensity of massive galaxies ranging from active SFGs to massive QGs in the SSA22 protocluster. This suggests that a red sequence has just begun appearing in this protocluster.

Uchimoto et al. (2012) discovered dense groups of massive galaxies as the counterparts of Ly α Blobs (LABs) and sub-mm galaxies (SMGs) in the SSA22 protocluster. Some of them are spectroscopically confirmed as plausibly physically associated groups in Kubo et al. (2016). Similarly, by

the abundance matching technique in a wide field survey, Vulcani et al. (2016) reported massive galaxies surrounded by many companions at high redshift as the progenitors of ultra massive galaxies today. They are likely to be hierarchical multiple mergers at the early-phases of the formation histories of massive ETGs, predicted from the high resolution cosmological numerical simulations in the Λ CDM Universe (e.g., Meza et al. 2003; Naab et al. 2007) and thus excellent laboratories of morphological evolutions of massive ETGs.

We here present the deep and high resolution imaging of an extremely dense group of galaxies at the core of the SSA22 protocluster, called the SSA22-AzTEC14 group, in the K' -band by using the InfraRed Camera and Spectrograph (IRCS; Kobayashi et al. 2000) and the Adaptive Optics system AO188 (Hayano et al. 2010) on Subaru Telescope. Since the $F160W$ -band of Hubble Space Telescope (*HST*), is too blue to study stellar morphologies in the rest-frame optical of galaxies at $z > 3$, an AO assisted K -band (rest-frame V -band) imaging with a 10-m class ground-based telescope is the best option for our targets. We describe the observation in Section 2. In Section 3, we report morphologies of galaxies in the AzTEC14 group. We discuss the environmental dependence of morphologies of massive QGs and SFGs, and behaviors of faint galaxies in the group in Section 4. In this paper, cosmological parameters of $H_0 = 70 \text{ km s}^{-1} \text{ Mpc}^{-1}$, $\Omega_m = 0.3$ and $\Omega_{\Lambda} = 0.7$ are assumed. In this cosmology, 1 arcsec corresponds to 7.633 kpc in physical at $z = 3.09$. We adopt the Chabrier (2003) Initial Mass function (IMF). The AB magnitude system is used throughout this paper.

2 OBSERVATION

Our target is an extremely dense group of galaxies found at the core of the SSA22 protocluster at $z = 3.09$, called the SSA22-AzTEC14 group (Kubo et al. 2016). Fig. 1 shows its combined image of the IRCS-AO K' (red) and *HST* $F814W$ (blue, here after *HST* I_{F814W})-band images. The object IDs are the same as those in Kubo et al. (2016) and Umehata et al. (2017). The AzTEC14 group was first discovered as a rare overdensity of distant red galaxies (DRGs; $J - K > 1.4$) at the position of a bright 1.1 mm source found from the ASTE/AzTEC 1.1 mm survey of the SSA22 field (Tamura et al. 2009; Umehata et al. 2014) by Uchimoto et al. (2012). In Kubo et al. (2016), we spectroscopically confirmed that seven galaxies belong to one group at $z_{\text{spec}} \approx 3.09$. Note that there is a large redshift uncertainty for Az14-K15c as its redshift was measured with the Balmer / 4000 Å breaks of its continuum spectrum. Five of them have stellar masses $M_{\star} > 10^{10.5} M_{\odot}$ and five of them are classified as DRGs. Comparing the AzTEC14 group with the galaxy formation models based on the Millennium simulation (Springel et al. 2005), we found that this group has properties similar to those of a dense group of galaxies at high redshift which evolves into a brightest cluster galaxy (BCG) of one of the most massive clusters in the current Universe (Kubo et al. 2016). Moreover, we carried out deep observations of this region at sub-mm by using Atacama Large Millimeter/submillimeter Array (ALMA) with a synthesized beam of $0''.70 \times 0''.59$ and a typical rms level of $60 \mu\text{Jy beam}^{-1}$ (green contours in Fig. 1, Umehata et al.

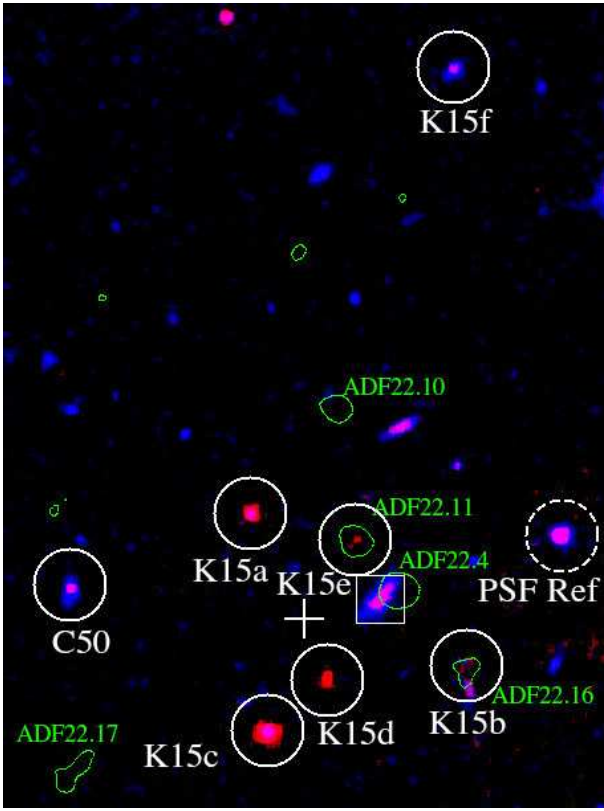


Figure 1. The combined image of the IRCS-AO K' (red) and HST/ACS I_{F814W} (blue)-band images of the AzTEC14 group ($20''.0 \times 27''.0$). The white circles show the objects with spectroscopic redshifts $z_{\text{spec}} \approx 3.09$. The object IDs are the same as those in Kubo et al. (2016) and Umehata et al. (2017). The white cross shows the coordinate of the LGS set in our operation. The dashed white circle shows the PSF reference star adopted in this study. The green contours indicate the 1.1 mm sources detected above 3σ per pixel on the image corrected with ALMA by Umehata et al. (2017). The white square shows the spectroscopically confirmed outlier.

2015; Umehata et al. 2017). The 1.1 mm fluxes of five sub-mm sources detected in the AzTEC14 group range from $S_{1.1 \text{ mm}} = 0.6$ to 2.0 mJy. ADF22.4 in Fig. 1 is newly confirmed at $z_{\text{spec}} = 3.091$ by detecting the redshifted CO(9-8) emission line (Umehata et al. 2017) and [C II] $158 \mu\text{m}$ (Hayatsu et al. submitted). Then now eight galaxies are confirmed as a dense group of galaxies at $z_{\text{spec}} \approx 3.09$.

Our high resolution near-infrared (NIR) imaging observation of the AzTEC14 group was conducted on 24, July 2015 by using the IRCS and AO188 equipped on Subaru Telescope (S15A-059; PI Mariko Kubo). The IRCS was used in the 52 mas plate scale mode with 54 arcsec field of view, and with the K' -band filter. The AO188 was operated in the laser guide star AO (LGS AO) mode. The tip tilt guide star (TTGS) for the LGS AO operation is a star with $R = 18.0$ at (R.A., Dec) = (22:17:35.78 +00:19:16.3) which is 52 – 64 arcsec apart from the targets. The exposure time was 2.8 hours in total. We reduced the data using the IRAF data reduction tasks following the data reduction manual for the

IRCS¹. The individual frames were combined after masking the bad pixels, flat fielding, sky subtraction and estimating the dither offsets in a standard manner. The zero-point magnitude of our IRCS-AO K' -band image is calibrated to that of our MOIRCS K_s -band image.

Thanks to the good observing condition, the AO works well despite the use of a faint and distant TTGS. The FWHM of the Point Spread Function (PSF) size at the PSF reference star (the dashed white circle in Fig. 1) is $\approx 0''.16$ while that in our previous MOIRCS imaging at this field is $\approx 0''.41$. The 5σ limiting magnitude measured with $0''.3$ and $1''.1$ diameter apertures on our IRCS-AO K' -band image are $K = 25.49$ and 23.51, respectively while that measured with an $1''.1$ diameter aperture on our MOIRCS K_s -band image is $K = 24.3$. Thus, for galaxies extended over $1''.1$ (≈ 8 kpc), detection completeness on our IRCS-AO K' -band image is lower than that on our MOIRCS K_s -band image.

We also show the archival I_{F814W} -band image taken with the Advanced Camera for Surveys (ACS) on the HST (PID 9760; PI Roberto Abraham). The FWHM of the PSF size on the I_{F814W} -band image is $0''.08$ and the 5σ limiting magnitude measured with a $0''.3$ diameter aperture is $I_{F814W} = 28.3$.

3 RESULTS

Figure 2 shows the IRCS-AO K' , HST/ACS I_{F814W} and MOIRCS K_s -band images of the galaxies in the AzTEC14 group. We also show the images at the position of ADF22.10 though it has not yet been spectroscopically confirmed as a group member. The red contours on the I_{F814W} -band stamps show the regions detected above 2σ per pixel on the IRCS-AO K' -band image. The green contours show isophotal areas of the 1.1 mm sources same as Fig. 1. The bottom right end rows show the stacks of the Az14-K15b, d, e, f and C50, the members classified as SFGs in § 3. 1. We mistook the object ID C50 as MD048 in the previous paper. Before stacking the images, the image centres are aligned at the centroids of the objects on the IRCS-AO K' -band image or MOIRCS K_s -band image if they are not detected on our IRCS-AO K' -band image. Both the K -band images are combined in median after matching their scales based on their total magnitudes measured on our MOIRCS K_s -band images. The I_{F814W} -band images are combined without any scaling since many of the group members are hard to be identified on the I_{F814W} -band images individually.

It is interesting that a wide variety of galaxies are observed within such a small volume. Even if we focus on only the galaxies with $M_\star \sim 10^{11} M_\odot$, they have a wide variety in morphologies, similar to a dense cluster reported in Wang et al. (2016) recently. Such extremely dense groups at high redshift are interesting laboratories maybe just at the transition epoch of morphologies.

Many of the members are hardly detected on the I_{F814W} -band image maybe owing to their red colors. Therefore the AO-assisted high-resolution K -band imaging is essential to study morphologies of such red galaxies at $z > 3$.

¹ http://www.subarutelescope.org/Observing/DataReduction/Cookbooks/IRCSimg_2010jan05.pdf

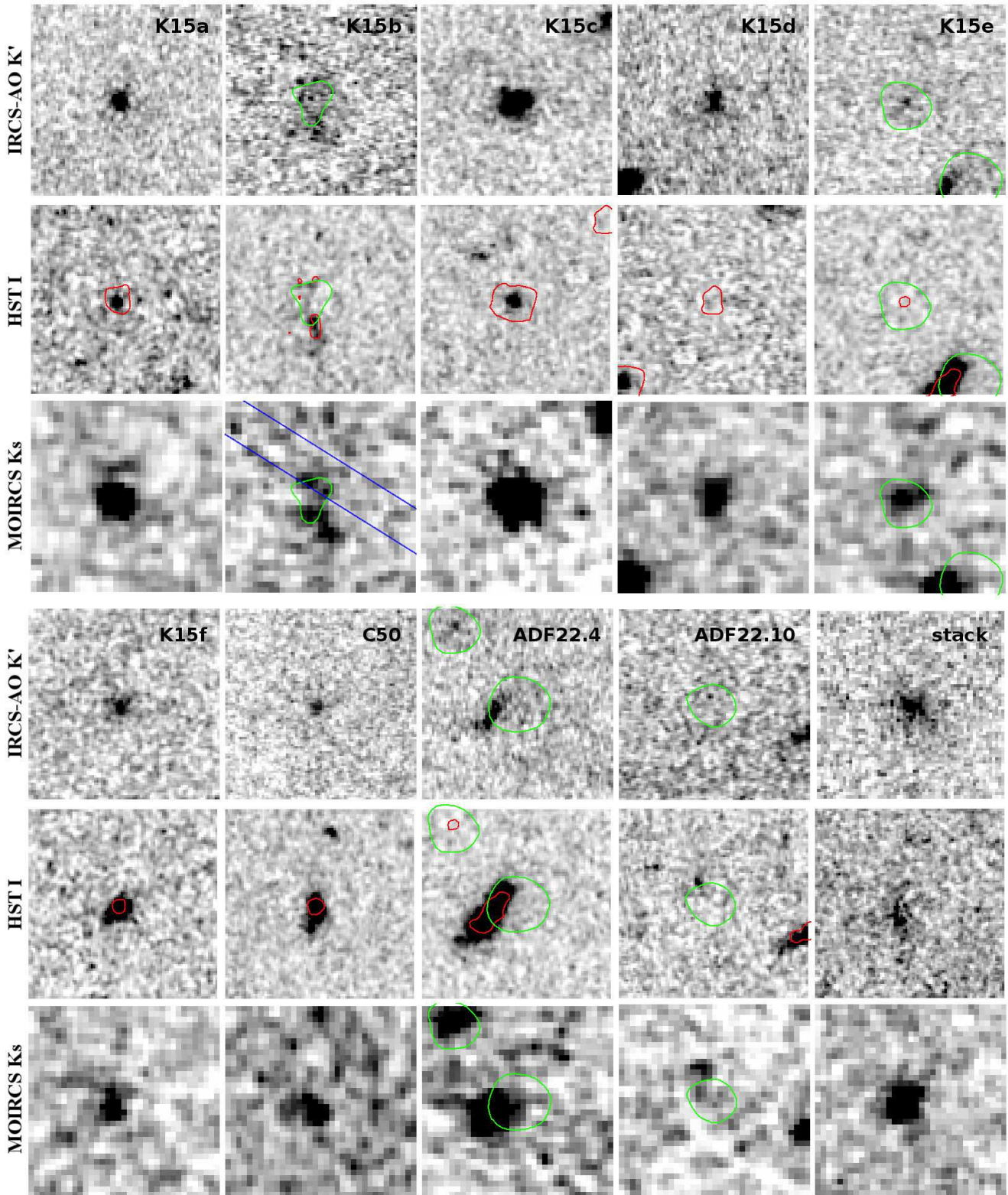


Figure 2. The *top*, *middle* and *bottom* rows show the IRCS-AO K' , *HST*/ACS I_{F814W} and MOIRCS K_s -band images of members of the AzTEC14 group, respectively ($4''.1 \times 4''.1$). The object IDs are the same as those in Fig. 1. We show the stacked images of SFGs (Az14-K15b, K15d, K15e, K15f & C50) at the right-bottom-end panels. The red contours shown in the *middle* rows are isophotal areas of the sources detected on the IRCS-AO K' -band image above 2σ per pix. The green contours show isophotal areas of the 1.1 mm sources detected with ALMA above 3σ (Umehata et al. 2017). The blue solid lines drawn on the MOIRCS K_s -band image of Az14-K15b show the slit position of our MOIRCS spectroscopy of this object (Kubo et al. 2015).

Table 1. GALFIT Morphological Parameters

Object	K_{tot} (mag)	M_* ($10^{10} M_{\odot}$)	r_e (kpc)	Sérsic n	b/a	PA (deg)	χ^2/dof
Az14-K15a	22.50 ± 0.10	$8.0^{+5.7}_{-2.9}$	1.37 ± 0.75	9.5 ± 4.5	0.58 ± 0.09	-61 ± 8	1.18
Az14-K15a (AGN-subtracted)			4.26 ± 0.60	2.2 ± 0.6	0.60 ± 0.09	-62 ± 12	1.18
Az14-K15c	21.55 ± 0.04	$25.4^{+7.3}_{-5.8}$	1.01 ± 0.04	2.5 ± 0.2	0.89 ± 0.03	-5 ± 11	1.10
Az14-K15d	23.06 ± 0.16	$5.3^{+5.7}_{-2.9}$	3.23 ± 1.56	4.6 ± 1.8	0.35 ± 0.07	85 ± 4	1.06
Az14-K15e	23.35 ± 0.21	$7.2^{+9.8}_{-5.2}$	11.9 ± 27.1	7.3 ± 8.9	0.09 ± 0.05	35 ± 3	1.07
Az14-K15f	23.30 ± 0.20	$1.7^{+2.2}_{-0.8}$	1.76 ± 0.32	1.3 ± 0.4	0.90 ± 0.12	-10 ± 52	0.91
C50	24.09 ± 0.37	$1.1^{+1.1}_{-0.7}$	1.84 ± 1.24	3.9 ± 2.8	0.64 ± 0.19	78 ± 20	0.99

Interestingly, some galaxies are more clearly detected on our MOIRCS K_s -band image (K15b and K15e in Fig. 2) while the point source sensitivity of our IRCS-AO K' -band image is better than that of our MOIRCS K_s -band image. We test the dependence of detection completeness on source morphology in § 3.3.3.

3.1 Morphologies and stellar populations

At first, we classify the members into QGs and SFGs from their rest-frame UVJ colors and SEDs. Fig. 3 shows $J - K$ v.s. $K - [4.5]$ or rest-frame UVJ color diagram (Williams et al. 2009). Aperture corrected photometries of each galaxies are performed by the way same as that in Kubo et al. (2013) but here we subtract spectroscopically measured $H\beta$ and $[\text{OIII}] \lambda\lambda 5007$ emission line fluxes from their K -band fluxes. In Kubo et al. (2016), we showed their observed and best-fit model SEDs at the u^* , B , V , R , i' , z' , J , H , K , 3.6, 4.5, 5.8 & 8.0 μm -bands obtained by fitting the observed flux values to the stellar population synthesis models of the Bruzual & Charlot (2003) adopting the Chabrier (2003) Initial Mass Function.

The two brightest members, Az14-K15a and K15c, satisfy the rest-frame UVJ color criterion of QGs and also have SEDs well characterized as those of QGs (Kubo et al. 2016). Other galaxies are classified as SFGs: C50 looks satisfying QG color criterion but there is large uncertainty in its rest-frame UVJ color. Looking its overall SED shown in Kubo et al. (2016), C50 has a blue color like a young SFG. Note that $K - [4.5]$ colors of Az14-K15d and K15e suffer from deblendings with adjacent sources at 4.5 μm . They can satisfy QG color criterion but are too faint to solve degeneracies of QG/SFG by SED fittings with our current data.

Following previous studies, we evaluate morphological properties by using the GALFIT (Peng et al. 2002, 2010). The GALFIT fits two-dimensional analytical functions convolved with an PSF to observed galaxy images. We use a star with $K = 22.6$ at (R.A., Dec) = (22:17:36.608, +00:18:22.52), which is 54, 9 and 5 – 16 arcsec apart from the TTGS, LGS and targets, respectively, as a PSF reference star (the dashed white circle in Fig. 1). We fit the Sérsic models (Sérsic 1968) with effective radii $r_e = 0.2 - 12$ kpc and Sérsic index $n = 0.5 - 10$. Fittings are performed for within two arcsec square regions of each object. Sky background values are estimated at the areas 1.5 to 2.0 arcsec apart from each object before Sérsic model fittings. We initially input total magnitudes measured by using the SExtractor (Bertin & Arnouts 1996) and typical morphological

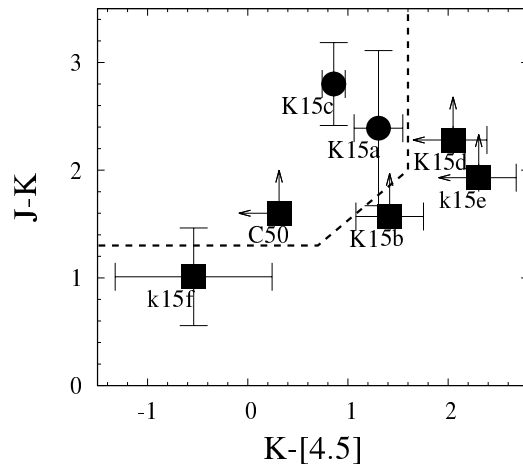


Figure 3. $J - K$ v.s. $K - [4.5]$ or rest-frame UVJ color diagram of galaxies in the AzTEC14 group. The black dashed line shows the rest-frame UVJ color criterion for QGs in previous studies. The black filled circles and squares show the galaxies classified as QGs and SFGs in the AzTEC14 group, respectively. C50 looks satisfying QG color criterion but there is a large uncertainty in its rest-frame UVJ color. K15d and K15e suffer from deblendings with adjacent sources on the 4.5 μm -band image.

parameters for $z \sim 3$ galaxies, $r_e = 1$ kpc and $n = 1.4$. We summarize the morphological properties obtained by using the GALFIT in Table 1.

Since there are large uncertainties in the morphological parameters estimated with the GALFIT except for those of the brightest one, we supplementary compare observed central to total flux ratios with those of models in Fig. 4. We take the 1 kpc radius aperture fluxes measured on the IRCS-AO K' -band image as central fluxes. Here we use the Kron fluxes measured on the MOIRCS K_s -band image by using the SExtractor as total fluxes since up to 90% of total fluxes of the galaxies in the AzTEC14 group measured on our MOIRCS K_s -band image are under the surface detection limit on our IRCS-AO K' -band image. We show the 2σ rms ranges of model flux ratios similarly measured on mock galaxy images in both the K -band from a thousand iteration for each. The two brightest members, Az14-K15a and Az14-K15c, have flux ratios similar to those of compact objects with $r_e \sim 1$ kpc. On the other hand, except for the faintest one, SFGs have flux ratios lower than those of compact objects with $r_e \sim 1$ kpc, i. e., more extended than

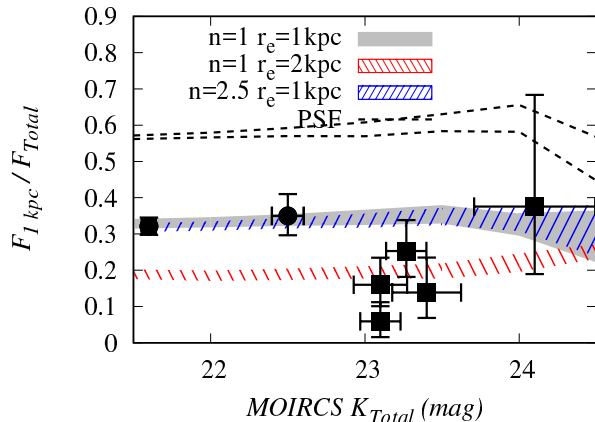


Figure 4. The ratios between central 1 kpc aperture radius fluxes measured on our IRCS-AO K' -band image and total fluxes measured on our MOIRCS K_s -band image as a function of total magnitudes measured on the MOIRCS K_s -band image. The galaxies classified as QGs and SFGs are shown with black filled circles and squares, respectively. The gray and red dashed regions show the Sérsic models with $n = 1$ and $r_e = 1$ & 2 kpc within 2σ rms ranges, respectively. Model flux ratios are properly calculated in the same manner as observed flux ratio estimated from both the K -band images. The blue dashed region is similar to gray dashed region but for a model with $n = 2.5$ and $r_e = 1$ kpc. The area between the black dashed lines shows a point source.

typical SFGs at $z \sim 3$. These results support the results of morphological analysis with the GALFIT in the following.

3.1.1 Quiescent galaxies

Figure 5 shows the size-stellar mass distribution of galaxies in the AzTEC14 group. QGs are shown with black filled circles. We also plot the size-stellar mass relations of SFGs and QGs at $z \sim 0$ and $z \sim 3$ in vdW14 and S15, both obtained by using the Cosmic Assembly Near-infrared Deep Extragalactic Legacy Survey (CANDELS; Grogin et al. 2011; Koekemoer et al. 2011) and 3D-HST (Brammer et al. 2012) data. Comparison with other studies is done by consistent way; We compare the results in circularized effective radii and stellar masses measured adopting the Chabrier IMF; The galaxies in vdW14 and S15 are selected based on the spectroscopic and photometric redshifts, and classified by the rest-frame UVJ color criterion; Morphological parameters in vdW14 and S15 are mainly evaluated by using the HST $F125W$ & $F160W$ -band images. In S15, SFGs at $z = 3$ are studied by using the rest-frame UV data but they reported that morphological k -correction for them is less than 20%.

The Sérsic indices and effective radii of the QGs, Az14-K15a and -K15c are $n = 9.5 \pm 4.5$ and $r_e = 1.37 \pm 0.75$ kpc, and $n = 2.5 \pm 0.2$ and $r_e = 1.01 \pm 0.04$ kpc, respectively. Fig. 6 shows the observed, model and residual images of Az14-K15a and Az14-K15c obtained by using the GALFIT. We show radial profiles of Az14-K15a and -K15c in the *central* and *left* panels of Fig. 7. Az14-K15c is well characterized as a massive compact elliptical similar to QGs found at $z > 1$ (e.g., Daddi et al. 2005; Trujillo et al. 2006, 2007; Toft et al.

2007; van Dokkum et al. 2008, 2010; Damjanov et al. 2009) but there is an matter of concern for Az14-K15a; it has an X-ray detected AGN detected with *Chandra* (Lehmer et al. 2009) which can sharpen its radial profile.

Since it is hard to resolve an AGN from a high redshift galaxy spatially with current instruments, here we deal with the AGN component of Az14-K15a assuming that AGN to stellar flux ratio is comparable to emission line to continuum flux ratio at K -band. Fig. 8 shows a spectrum and spatial extent of the [OIII] λ 5007 of Az14-K15a obtained in Kubo et al. (2015). It has double peaks in spectral direction but is just an point like source in spatial direction. The [OIII] λ 5007 line width and fluxes of the shorter and longer wavelength peaks are $\sigma = 225 \pm 11$ km s $^{-1}$ and $19.1 \pm 0.7 \times 10^{-17}$ erg cm $^{-2}$ s $^{-1}$, and 102 ± 17 km s $^{-1}$ and $6.5 \pm 0.8 \times 10^{-17}$ erg cm $^{-2}$ s $^{-1}$, respectively. Together with H β and [OIII] λ 4959, emission line flux contribute to about 30% of the K -band flux. Then we re-fit the Az14-K15a to models composed from a point source and a Sérsic model with a fixed flux ratio of 3 : 7, assuming that all the emission line flux shifted in the K -band is originated in AGN(s) (central point source) and all the continuum emission comes from the stellar component (Sérsic model). Note that the influence of such a nuclear component is negligible for Az14-K15c since no signature of an AGN is detected and upper limit of the contamination of the [OIII] to the K -band flux is less than 1% in Az14-K15c from our spectroscopic observations in Kubo et al. (2015).

The Sérsic indices and effective radii of the best-fit Sérsic model of double-components fit are $n = 2.2 \pm 0.6$ and $r_e = 4.3 \pm 0.6$ kpc. The green thin and thick long dashed lines in the *central* panel of Fig. 7 show the best-fit models of a point source and Sérsic model, and the sum of the two models. The model and residual images of the single and double components fits are shown in the *second* and *third* panels of Fig. 6. Both fits looks very similar but at a large scale, observed radial profile is reproduced better by double-components model.

From these above, we found that one of the two QGs in the AzTEC14 group is as compact as field one at $z \sim 3$ while other one is as large as giant elliptical at $z = 0$, though there is large uncertainty in the latter one. It is reported that QGs in protoclusters have sizes larger than those in general fields at $z < 2$, implying accelerated size growths of them in overdense regions, possibly by enhanced merger rates (Zirm, Toft, & Tanaka 2012; Cooper et al. 2012; Papovich et al. 2012; Lotz et al. 2013; Newman et al. 2014; Andreon, Dong, & Raichoor 2016). At first, our results challenge the reliability of past studies arguing compact morphologies of QGs at high redshift without NIR spectroscopic follow-ups. In case of the SSA22 protocluster, now five, about a third of the candidate QGs selected in Kubo et al. (2013) are spectroscopically confirmed as the protocluster members in Kubo et al. (2015). Except for Az14-K15c, they are X-ray detected and confirmed by detecting their redshifted [OIII] λ 5007 or Ly α emission lines plausibly originated in AGNs, similar to Az14-K15a. Other studies also report that AGNs are frequently seen among massive QGs at $z > 2$ (Olsen et al. 2013; Marsan et al. 2016). On the other hand, some massive compact ellipticals at high redshift are certainly found like Az14-K15c and in other studies by deep spectroscopic observations (e.g., van Dokkum et al. 2008). Further studies of morphologies

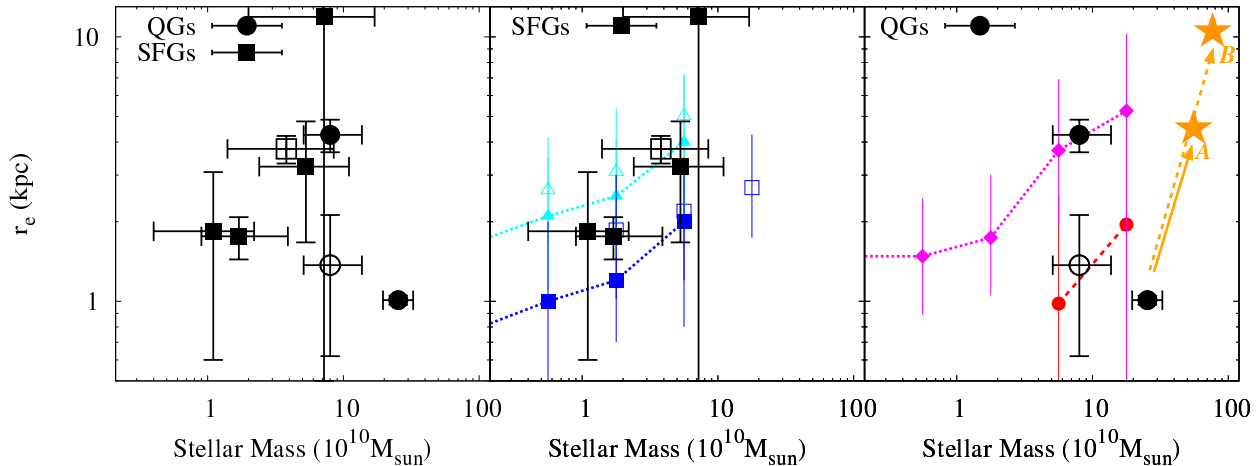


Figure 5. *Left:* The effective radius (r_e) to stellar mass relation. The black filled circles and squares show the QGs and SFGs in the AzTEC14 group, respectively. The large black open square shows the stack of the SFGs. The large black open circle shows the result of a single Sérsic fit of Az14-K15a. *Central:* Focusing on SFGs. The cyan filled triangles and small blue filled squares with dot lines show SFGs at $z = 0$ and $z = 3$ from S15, respectively. The cyan open triangles and small blue open squares show SFGs at $z = 0.25$ and $z = 2.75$ from vdW14, respectively. *Right:* Focusing on QGs. The magenta filled diamonds with dot line and small red filled circles with dot line show QGs $z = 0$ and $z = 3$ from vdW14, respectively. The orange stars at the point of the arrows are the expected sizes and stellar masses of Az14-K15c at $z \sim 1$ in cases all the members merge into this object without (Case A) or with (Case B) in situ star formation.

properly dealing with AGN components are required to conclude when giant ellipticals appeared in cluster of galaxies.

It should be noted that [OIII] λ 5007 emission line of Az14-K15a at shorter wavelength has a wing at the upper side with respect to the centre (Fig. 8). Since no such component is detected on both the K-band images, this wing component should have a large [OIII] λ 5007 equivalent width like Ly α Blobs. This wing component extends to $\sim 1'' \sim 8$ kpc, much more larger than the typical size ($r_e = 1 \sim 2$ kpc) of galaxies at $z \sim 3$. We will discuss the origin of this extended and double peaked [OIII] λ 5007 emission lines in § 4. 2.

3.1.2 Star forming galaxies

The SFGs except for Az14-K15b and ADF22.4 are shown with black filled squares in Fig. 5 while Az14-K15b is too diffuse to obtain a reasonable fit and ADF22.4 is not significantly detected on the IRCS-AO K' -band image. The stack of the SFGs is shown with the black open square. Except for the lowest stellar mass one, they tend to be larger than normal SFGs at the same redshift. In addition, the region detected over 2σ per pixel of Az14-K15b ($M_* \approx 10^{11} M_\odot$) is extended to $1''.5$ (≈ 11.5 kpc) at least. Although these SFGs are too faint ($K = 23.1 \sim 24.1$) to constrain their morphological parameters robustly, it is interesting that massive SFGs are all above the size-stellar mass relation of field galaxies. The simple photometric analysis in Fig. 4 also supports this tendency.

The *right* panel of Fig. 7 shows the radial profile of stack of the SFGs in the AzTEC14 group compared with the stacks of model galaxies in a range of typical galaxies at $z \sim 3$. We simulate stacked images by stacking five model galaxies with magnitude distributions same as that of the

SFGs in the AzTEC14 group and morphological parameters randomly scattered in ranges of $r_e = 0.5 - 2$ kpc, $n = 0.5 - 4$, axis ratio $0 \sim 1$ and position angle $0 \sim 90$. The black dashed line and gray shaded region show the median and 2σ rms around the median of radial profiles of the stacks of model galaxies. The radial profile of stack of the SFGs in the AzTEC14 group is flatter than those of the model stacks of typical $z \sim 3$ galaxies, i.e., the observed radial profile cannot be reproduced unless they are dominated by galaxies with $r_e > 2$ kpc. From these above, we conclude that massive SFGs in the AzTEC14 group have the sizes on average larger than those of typical SFGs at $z \sim 3$.

The difference in the size-stellar mass relation between SFGs in the AzTEC14 group and in general fields is likely to be originated in the sample bias since SFGs in the AzTEC14 group are classified as DRGs, namely rare massive dusty starburst galaxies. The size-stellar mass distribution of our sample is similar to that of massive H α emitters (HAEs) at $z = 2.5$ (Tadaki et al. 2014). In their study, low mass HAEs are on the size-stellar mass relation of normal SFGs at similar redshift while massive HAEs are on the size-stellar mass relation of SFGs at $z = 0$. They searched HAEs at $z = 2.5$ in general fields by using a narrow-band filter but the strong spatial clustering of HAEs implies that they are plausible progenitors of massive ETGs in clusters or groups, similar to the SFGs in the AzTEC14 group.

The environmental dependence of morphologies of LBGs is discussed in many studies while the galaxies studied here are biased to DRGs, which do not often overlap with LBGs (Kubo et al. 2013). We found no significant difference between C50, classified as a LBG, and field galaxies at $z \sim 3$, similar to Peter et al. (2007) and Overzier et al. (2008) while Hine et al. (2016) reported the enhanced merger fraction among the LBGs in the SSA22 protocluster. These stud-

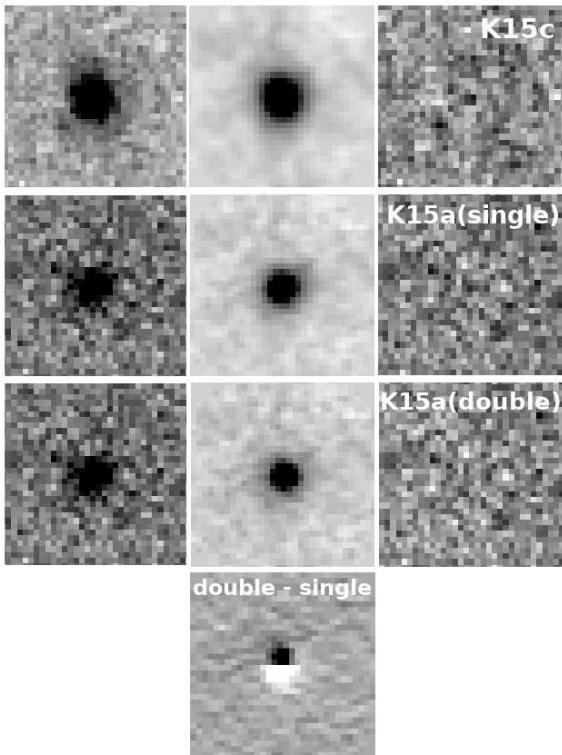


Figure 6. Examples of the Sérsic model fittings of Az14-K15c (*first row*) and Az14-K15a (*second row*: single Sérsic model and *third row*: double-components model). The observed images, best-fit Sérsic models and residuals from left to right. The sizes of the images are $1''.7$ square. The *bottom row* shows the double-components model subtracted of single Sérsic model. The scale is changed from the top three panels to emphasize differences.

ies used the images at rest-frame UV. Further observations at rest-frame optical may be also needed to discuss the environmental dependence of galaxy morphologies. On the other hand, Peter et al. (2007) reported that DRGs have relatively wide range of morphological parameters and include more high multiplicity objects and compact objects compared to LBGs. The environmental dependence of galaxy morphologies is still controversial, but at least, we can argue that DRGs, strongly clustered massive galaxies or plausible progenitors of massive ETGs today, have morphologies different from LBGs.

3.1.3 Sub-mm sources

Ikarashi et al. (2015) reported a median circularized sizes of $r_e \sim 0.67$ kpc for bright SMGs measured at NIR, which is comparable to the effective radii of compact ellipticals at $z = 2 - 3$. On the other hand, (Rujopakarn et al. 2016) reported that relatively faint ($S_{1\text{ mm}} \lesssim 1$ mJy) sub-mm sources at $z = 2 - 3$ have the sizes of $r_e \sim 4 - 5$ kpc at sub-mm in median, comparable to those of their stellar contents.

There are five moderately luminous ($S_{1\text{ mm}} \sim 1$ mJy) sub-mm sources identified by using ALMA at the AzTEC14 group and three of them are spectroscopically confirmed at $z_{\text{spec}} \approx 3.09$. We show the stamps of four out of the five sub-mm sources (K15b=ADF22.16, K15e=ADF22.11, ADF22.4

and ADF22.10) in Fig. 2 while no significant counterparts are detected for the rest one, ADF22.17, in all the I_{F814W} and K -bands. The green contours in Fig. 2 show the isophotal contours of the 1.1 mm sources detected above 3σ per beam. The blue solid lines of Az14-K15b in Fig. 2 show the slit with $0''.8$ width used in our MOIRCS spectroscopy. As the alignment accuracy of MOIRCS is better than 0.1 arcsec rms², we might confirm the stellar component at the north of the sub-mm source and/or the sub-mm source itself. The bright object detected near ADF22.4 is a galaxy confirmed at $z_{\text{spec}} \approx 0.57$ (Kubo et al. 2015) and ADF22.4 can be lensed by this object.

Although the K' -band counterparts of the sub-mm sources are too faint to constrain the robust morphological parameters with the GALFIT, there are several clues suggesting that they have spatially extended stellar components; Az14-K15b is extended to $1''.5$ (≈ 11.5 kpc). The $\approx 85\%$ of the total flux of Az14-K15e is lost on our IRCS-AO K' -band image and possible counterparts of ADF22.4 and ADF22.10 are detected on our MOIRCS K_s -band image but not detected on our IRCS-AO K' -band image. The influence of morphologies on detection completeness and measured total flux values on our IRCS-AO K' -band image are described in Appendix C. Large sizes of them can cause such poor detections on our IRCS-AO K' -band image. In Umehata et al. (2017), it is reported that the deconvolved angular size of ADF22.4 is 1.9 ± 0.4 kpc in FWHM and those of other sub-mm sources in the SSA22 protocluster are 2 – 3 kpc though the spatial resolution and signal to noise ratio are not enough to show whether they have remarkably compact or not. At this point, it is not also clear whether there is a segregation between the morphologies in sub-mm and rest-frame optical.

3.2 Deficiency of low mass galaxies

Stellar mass function is one of the key properties to characterize a group of galaxies. Deep K -band images are useful to constrain stellar mass function of galaxies at $z > 3$. In our previous study with MOIRCS (Kubo et al. 2016), we show that stellar mass function of the AzTEC14 group is consistent with those of proto-BCG groups at $z \sim 3$ predicted from the galaxy formation models based on the Millennium simulation (Springel et al. 2005; De Lucia & Blaizot 2007; Guo et al. 2011) at above $M_* \geq 4 \times 10^{10} M_\odot$.

Given the empirical size-stellar mass relation at $z \sim 3$ in general fields, galaxies with stellar masses below the above completeness limit have sizes smaller than 1 kpc ($\approx 0''.1$) in typical. If so, our new IRCS-AO K' -band image could give further constraints on stellar mass function of the AzTEC14 group; the completeness limit downs to $M_* \gtrsim 10^{10} M_\odot$ and the 20 \sim 40% of galaxies with $M_* = 10^{9.5} \sim 10^{10} M_\odot$ are expected to be detectable on our IRCS-AO K' -band image. Then 5 \sim 20 new members should be detected if stellar mass function of the AzTEC14 group is continuously consistent with the above cosmological numerical simulations. However no additional member is detected in our IRCS-AO K' -band image.

Detection completeness of galaxies depends on both

² http://subarutelescope.org/Observing/Instruments/MOIRCS/spec_mos.html

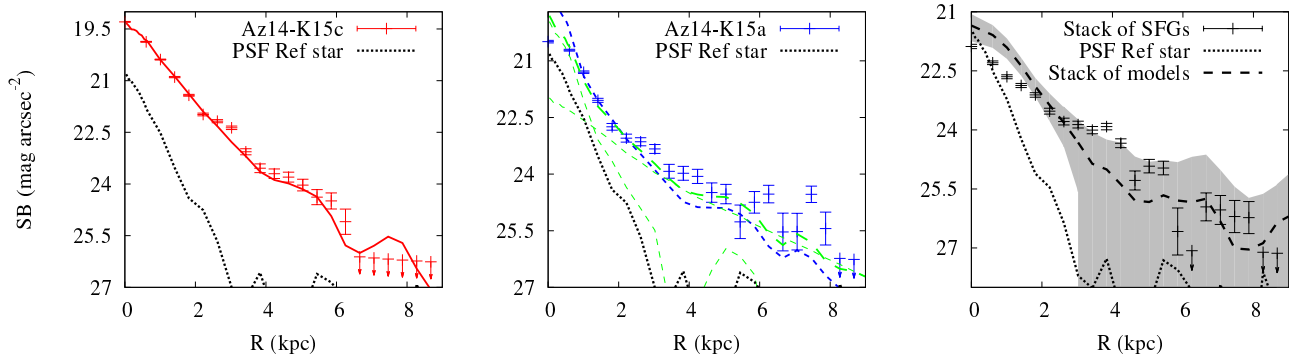


Figure 7. *Left:* The red crosses and solid line show the observed radial surface brightness profile and its best-fit model of Az14-K15c. The black dot line shows the radial profile of the PSF reference star. *Center:* The blue crosses and thick dashed line show the observed radial surface brightness profile and its best-fit model by a single Sérsic model fitting of Az14-K15a. The green thick long dashed line shows the best-fit model of the combination of a point source and Sérsic model. The green thin dashed lines show a point source and Sérsic model combined in the green thick long dashed line. *Right:* The black crosses show the radial surface brightness profile of a stack of the IRCS-AO K' -band images of the SFGs in the AzTEC14 group with 2σ errors. The black dashed line and gray shaded region show the median and 2σ rms around the median of the stacks of model galaxies with $r_e = 0.5 - 2$ kpc and $n = 0.5 - 4$, measured from a thousand times iteration.

colors and morphologies. The influence of colors as red as $J - K \sim 2$ is already included in the above stellar mass completeness limit. Given that many of galaxies in the AzTEC14 group have sizes larger than typical $z \sim 3$ galaxies, we cannot ignore the influence of source morphologies on detection completeness. MOIRCS K_s -band image may be also affected by source morphologies while our previous study ignored such an effect. We discuss stellar mass function of the AzTEC14 group in § 4. 5.

3.3 Fitting errors and detection completeness

In this section, we test the influence of PSF variation, reproducibility of morphological parameters with the GALFIT and detection completeness on our IRCS-AO K' -band and MOIRCS K_s -band images.

3.3.1 PSF variation

Since performance of an AO system depends on separations of targets from a LGS and TTGS, we need to concern the influence of PSF variation on estimating morphological properties. The separation between the LGS and the PSF reference star is 9 arcsec while those between the LGS and our targets range from 2 – 19 arcsec. According to the performance of the AO188³, the FWHM of the PSF size at Az14-K15d can be $\sim 10\%$ ($\sim 0''.02$) smaller than that at the position of the PSF reference star while those at Az14-K15a, K15c and K15e can be $\sim 5\%$ ($\sim 0''.01$) smaller and that at Az14-K15f can be 10% ($\approx 0''.02$) larger. The degradation of the performance owing to the separation from the TTGS is $\sim 1\%$ for our targets.

To see the influence of PSF variation, we compare results of the GALFIT obtained by using different PSF reference stars. Besides the PSF reference star adopted in

this study, three stars are observed simultaneously but the FWHMs of the PSF sizes measured from them are $0''.16$, $0''.17$ & $0''.18$. The separations of these stars from TTGS and LGS range 44 – 75 and 18 – 23 arcsec, respectively. We compare the Sérsic indices and effective radii estimated with these stars and the PSF reference star adopted in this study in Fig. A1. The influence of PSF variation on the estimated effective radii is small except for a galaxy with the largest effective radius among the group. On the other hand, the estimates of Sérsic indices vary greatly by PSF reference stars used.

Again, at Az14-K15c, the brightest and one of the key objects of this study, the PSF size is expected to be $\sim 5\%$ ($\sim 0''.01$) smaller than that at the PSF reference star adopted. In Fig. A1, use of $\sim 0''.01$ different FWHM PSF size changes the estimated Sérsic index and effective radius of Az14-K15c by only 0.5 and 0.2 kpc. Thus the results of Az14-K15c is not likely to be strongly affected by PSF variation, though ideally, we should also test of PSF references with PSF sizes smaller than that of the PSF reference star adopted in this study.

3.3.2 Performance of the GALFIT on our IRCS-AO K' -band image

Next, we test the performance of the GALFIT on our IRCS-AO K' -band image. To test the reproducibility of morphological parameters, we generate mock galaxy images by making model galaxy images convolved with the observed PSF profiles by using the GALFIT and putting them on the blank fields of the observed image to add the sky fluctuation. Then we re-run the GALFIT. We show the deviations of measured values from initial values in Fig. B2. Briefly, for typical compact elliptical galaxies at $z \sim 3$ ($n \geq 2.5$ and $r_e = 0.5 \sim 1$ kpc) with $K_{\text{tot}} = 22$ ($K_{\text{tot}} = 22.5$), the 1σ rms errors of the re-estimated values from the model parameters are $\sigma_{r_e} = 0.3$ (0.5) kpc and $\sigma_n = 1$ (3). For typical late-type galaxies at $z \sim 3$ ($r_e = 0.5 \sim 2$ kpc and $n < 2.5$) with

³ <http://www.naoj.org/Observing/Instruments/AO/performance.html>galaxies at $z \sim 3$ ($r_e = 0.5 \sim 2$ kpc and $n < 2.5$) with

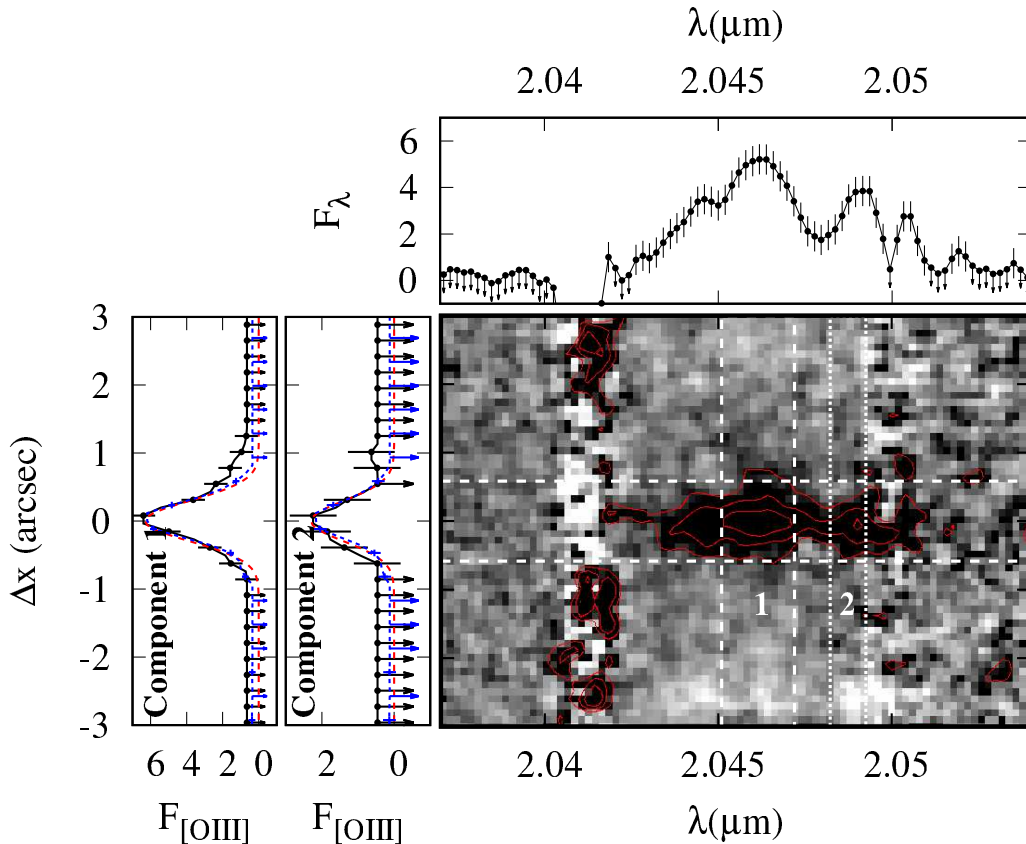


Figure 8. *Bottom right:* The spectral image of Az14-K15a around its [OIII] λ 5007 emission lines. The red contours are isophotal area detected above 1.5, 3 and 5 σ per pixel. *Top:* The black points with lines show one dimensional spectrum of Az14-K15a obtained by summing up the spectrum image in spatial direction for $\approx 1''.2$ between the horizontal white dashed lines in the spectral image. F_λ is in 10^{-18} erg cm $^{-2}$ s $^{-1}$ \AA^{-1} . *Bottom left:* The black points with lines show spatial extents of the spectrum at shorter (Component 1) and longer wavelength (Component 2) peaks obtained by summing up the spectral image for ≈ 14 & 7 \AA in spectral direction, between the white vertical dashed lines and dot lines in the central image, respectively. $F_{[\text{OIII}]}$ are in 10^{-18} erg cm $^{-2}$ s $^{-1}$ pix $^{-1}$ (1pix= $0''.117$). Component 2 is stacked avoiding adjacent OH sky emission. The blue dot lines and cross points show the spatial extent of Az14-K15a measured on the MOIRCS K_s -band image smoothed to have FWHM PSF size $0''.7$, typical FWHM PSF size of this spectroscopic observation. The fluxes within the slit expected from our observing plan of this spectroscopic observation, where slit width was $0''.8$, are summed up and scaled to match with the scale of spectra. The red dashed lines show a spatial extent of a point source with FWHM PSF size $0''.7$, similarly measured as the blue dot lines and crosses.

$K_{\text{tot}} = 22.5$ (24.0), the 1σ rms errors are $\sigma_{r_e} = 0.7$ (1.3) kpc and $\sigma_n = 0.4$ (1.9). For large late-type galaxies with $r_e = 3$ kpc and $K_{\text{tot}} = 22.5$ (24.0), the 1σ rms errors are $\sigma_{r_e} = 1.2$ (1.9) kpc and $\sigma_n = 0.4$ (2.8). For faint objects with $K > 22.5$ and $r_e > 4$ kpc, measured r_e are significantly underestimated. Sérsic indices of objects with $K > 22.5$ and/or large Sérsic indices suffer from large errors.

According to Table 1, and Fig. B2 and B1, we can obtain reliable morphological parameters for Az14-K15c with $K_{\text{tot}} = 21.6$ but other members may suffer from large errors. Az14-K15a is as bright as $K = 22.5$ but as we describe above, its K -band flux is pushed up by an AGN component. r_e of Az14-K15d, n of Az14-K15f could be trusted though both are not reliable for Az14-K15e. There are possible additional uncertainties originated in the substructures like AGNs and giant clumps frequently seen among massive galaxies at high redshift (e.g., Elmegreen & Elmegreen 2006; Genzel et al. 2006, 2008; S15; Shibuya et al. 2016). S15 re-

ported that the fraction of clumpy galaxies increases with redshift and becomes $\sim 50\%$ at $z \sim 2$. Multiple giant clumps are not clearly identified in our targets, may be due to the low signal to noise (S/N) ratio compared to previous studies with the *HST* but the different morphologies in different wavelength of Az14-K15b and C50 imply their complex structures.

3.3.3 Detection completeness

Here we test dependence of detection completeness on source morphologies by generating mock galaxy images by the way described in § 3.3.2 and extracting them by using the SExtractor. We extract sources detected over 1.5σ at each pixel (1 pix = $0''.052$ for IRCS and $0''.117$ for MOIRCS) for > 0.02 and > 0.2 arcsec 2 adjacent areas on the IRCS-AO K' and MOIRCS K_s -band images, respectively.

We show the detection completeness for models with $n = 1$ & 4.0 and $r_e = 1, 2,$ & 3 kpc in Fig. C1 & C2. Fig. C3 shows the completeness of measured total magnitudes. The detection completeness on our IRCS-AO K' -band image sharply drops as sources have large sizes. Objects with $K_{\text{tot}} < 24$ are almost completely detectable on our IRCS-AO K' -band image but their total magnitudes can be significantly underestimated. The detection completeness on our MOIRCS K_s -band image is less sharply but also affected by source morphologies.

4 DISCUSSION

4.1 Dense group of galaxies at high redshift

There are many dense groups of massive galaxies in the SSA22 protocluster, which are plausible evidences of formations of giant elliptical galaxies via hierarchical multiple mergers. Such galaxy groups are reported in other studies. A dense cluster at $z = 2.506$ (CL J1001) found by Wang et al. (2016) is similar to the AzTEC14 group in many aspects. The CL J1001 cluster has a collapsed halo with $M_{200c} = 10^{13.9 \pm 0.2} M_{\odot}$ and contains 11 massive galaxies within 80 kpc from the cluster centre ($M_{\star} \gtrsim 10^{11} M_{\odot}$ with the Salpeter IMF, corresponds to $M_{\star} \gtrsim 10^{10.5} M_{\odot}$ with the Chabrier IMF). They found no object comparable to the CL J1001 cluster in the Millennium simulation while the AzTEC14 group has only one comparable group at each $z \sim 3$ snapshot. The CL J1001 cluster and the AzTEC14 group are also similar in overdensities of DRGs, QGs, sub-mm sources and AGNs.

QGs and many SFGs in the CL J1001 cluster are compact while no massive compact SFG is seen in the AzTEC14 group. Several studies reported compact SFGs and sub-mm galaxies at high redshift (e.g., Simpson et al. 2015; Ikarashi et al. 2015; Tadaki et al. 2015) which can evolve into compact QGs by just quenching their star formation activities. The absence of compact SFGs in the AzTEC14 group can be owing to the short periods of compact SFG phases. We note that larger k -correction can be required in Wang et al. (2016) since they applied the morphological k -correction based on vdW14 but their sample is biased to red galaxies rarely seen in general fields like galaxies in the AzTEC14 group which show very different morphologies in rest-frame UV and optical (Fig. 2) and careful subtractions of nuclei components with strong [OII] emission lines can be required since many galaxies in the CL J1001 cluster show signatures of AGNs.

It is beyond the scope of this paper but it is surprising that such rare density peaks hardly seen in the volume of the current large cosmological numerical simulations are discovered by field surveys with limited volumes. Further large volume cosmological numerical simulations and wide field surveys of such dense groups are required to show the consistency of their simulated and observed properties.

4.2 Extended and double peaked [OIII] λ 5007 emission lines from a quiescent galaxy

Since Az14-K15a is a young QG, to be strict, post-starburst galaxy having the SED of ~ 0.5 Gyr after burst-like star for-

mation, footprints of its quenching process can be still observed. It is interesting that Az14-K15a is an AGN showing double peaked and spatially extended [OIII] λ 5007 emission lines.

Plausible origins of double peaked emission lines from an AGN(s) are dual AGNs, outflows and/or a rotating narrow line region (e.g., Müller-Sánchez et al. 2011, 2015). Since the two peaks have different line width, a rotating narrow line region scenario is ruled out. It is hard to resolve dual AGNs at $z > 3$ with current instruments but if double peaked [OIII] λ 5007 emission lines are originated in dual AGNs, it is a direct evidence of major mergers of galaxies (or giant stellar clumps) hosting a SMBH for each. Similarly, the objects with double peaked CO emission lines are seen in a protocluster at $z = 2.5$ (Tadaki et al. 2014) and a dense compact cluster of Wang et al. (2016), suggesting frequent gas rich mergers of galaxies in the protocluster environments.

An spatially extended metal emission line region is more likely to be produced by outflows rather than inflows of pristine gas. Thus the [OIII] λ 5007 of Az14-K15a is likely to be originated in outflows or a combination of outflows and dual AGNs. It is very interesting to find a plausible signature of outflows from an AGN(s) in a QG in a protocluster at $z > 3$. Similarly, [OIII] ([OII]) Blobs were found at $z = 1 \sim 1.6$ (Brammer et al. 2013; Yuma et al. 2013; Harikane et al. 2014). Further deep spatially resolved spectroscopy of Az14-K15a and other post-starburst galaxies in protoclusters may help us understanding how AGN activities relate with quenching of galaxies.

4.3 Evolution scenario of a BCG

Discovery of a massive compact elliptical, Az14-K15c, in such a proto-BCG group supports the two-phase formation scenario of giant elliptical galaxies that massive compact ellipticals formed at once and they evolve in sizes and stellar masses by series of mergers (e.g., Oser et al. 2010), which has also been supported by many observational studies (e.g., van Dokkum et al. 2010; Morishita et al. 2015; Zirm, Toft, & Tanaka 2012; Cooper et al. 2012; Papovich et al. 2012; Lotz et al. 2013; Newman et al. 2014; Andreon, Dong, & Raichoor 2016).

It is known that BCGs are on the size-stellar mass relation above that of non-BCGs (Bernardi et al. 2007; Bernardi 2009; Zhao, Aragón-Salamanca, & Conselice 2015). Several simulations (e.g., Laporte et al. 2013; Shankar et al. 2015) and observations (e.g., Lidman et al. 2013; Burke & Collins 2013; Zhao, Aragón-Salamanca, & Conselice 2015) argue that BCGs double their stellar masses between $z = 0$ to 1 while little growths of BCGs at $z < 2$ are reported in e.g., Collins et al. (2009), Stott et al. (2010, 2011). Recently, Zhang et al. (2016) reported a redshift-dependent BCG-cluster mass relation at up to $z \sim 1.2$. Az14-K15c needs to evolve in a size and stellar mass for > 10 and four times, respectively to evolve into a BCG hosted in one of the most massive clusters today ($M_{\text{cluster}} \sim 10^{15} M_{\odot}$ & $M_{\star, \text{BCG}} \sim 10^{12} M_{\odot}$) while size growths by factor ~ 5 from $z = 0$ to 3 are expected for compact QGs at $z > 2$ in typical (e.g., Toft et al. 2007; van Dokkum et al. 2008; Damjanov et al. 2009; van Dokkum et al. 2010; van der Wel et al. 2014).

We roughly estimate the size and stellar mass growths of

Az14-K15c assuming that all the group members will merge into this object. The size growth of an object by mergers can be written as $r_{g,f}/r_{g,i} = (1 + \eta)^2/(1 + \eta\epsilon)$, adopting the virial theorem following Naab, Johansson, & Ostriker (2009). $r_{g,f}$ and $r_{g,i}$ are the final and initial gravitational radii. η and ϵ are ratios of masses and mean square speeds of the stars, respectively, between accreting and initial objects. Here we assume that the velocity dispersion of each group member is similar to those of compact QGs at $z = 2 - 3$ which are 200 to 500 km s⁻¹ for galaxies with the stellar masses $M_* = 10^{10} - 2 \times 10^{11} M_\odot$, extrapolated from van Dokkum, Kriek, & Franx (2009) and Bezanson et al. (2009). The above formalism is hold in case of dry mergers. Note that if massive SFGs in the group are gas rich when they merge, the size growth of Az14-K15c by mergers can be suppressed (Welker et al. 2015).

All the galaxies in the AzTEC14 group can merge into one massive galaxy in 3 – 4 Gyr or by $z \sim 1$, according to the numerical simulations of compact groups (e.g., Barnes 1989; Bode, Cohn, & Lugger 1993) which have the dynamical timescales similar to the AzTEC14 group. If we just use the observed stellar mass values of the members at $z = 3.09$, the size and stellar mass of the final product are the 3 – 4 times and double of the initial values of Az14-K15c, respectively (Case A in Fig. 5). It is consistent with the simulations and observations predicting continuing strong size growths at $z < 1$. If the SFGs in the AzTEC14 group keep to be on or above the star formation main sequence for $\gtrsim 1$ Gyr before mergers, they can double their stellar masses and exhaust large fractions of gas. In such case, the size and stellar mass of the final product are 8 – 10 and four times of the initial values, respectively (Case B in Fig. 5). If Az14-K15c follows case B scenario and/or there are large extra accretion of galaxies, it could have already become a BCG today by $z > 1$.

Contributions of mergers of satellites to the evolution of a compact elliptical from $z = 2$ to 1 was discussed by using a deep *HST* image in Morishita & Ichikawa (2016). They argue that to reproduce the observed and simulated size growths of massive ETGs, not only just merging satellites but also in situ star formation in them are required. In case B, the net stellar mass increase by mergers is $\sim 20\%$ of the descendant galaxy at $z \sim 1$, similar to the results of Morishita & Ichikawa (2016). Note that further size and stellar mass growths by satellites are expected for Az14-K15c since some of the members of the AzTEC14 group are sub-mm galaxies which may more rapidly grow in stellar masses than galaxies on the star formation main sequence, much more accretions of satellites are expected at the core of a protocluster and the stellar mass completeness limit of our observations is not as small as Morishita & Ichikawa (2016).

We note that some mergers expected in the AzTEC14 group can have the stellar mass ratios categorized as major mergers. Multiple major mergers can form slow rotators frequently seen among the most massive ETGs like BCGs while minor and major binary mergers result in fast rotators (Moody et al. 2014).

4.4 Nascent red sequence galaxies

Not only compact QGs but also SFGs in protoclusters are plausible progenitors of massive ETGs today. According to

the model predictions, most of the members of the AzTEC14 group plausibly merge into one BCG in the current Universe but they still inform us how stars formed in galaxies at early time. Especially, massive SFGs in the AzTEC14 group are mostly classified as DRGs, known to show strong clustering (Quadri et al. 2007; Ichikawa et al. 2007), i.e., preferentially inhabiting in the environments where evolve into clusters or groups.

One plausible explanation for the large sizes of massive SFGs classified as DRGs is the differences in halo masses before their dark matter halos incorporate into one massive halo. The sizes and rotational velocities of galaxy discs follow the sizes and circular velocities of their host dark matter halos. It is known that DRGs show strong clustering (Quadri et al. 2007; Ichikawa et al. 2007). More strongly clustered galaxies are hosted in more massive dark matter halos. Based on the clustering analysis, Quadri et al. (2007) reported the halo mass $M_H \sim 5 \times 10^{12} M_\odot$ and $M_H \sim 2 \times 10^{13} M_\odot$ for photo-z or spec-z selected galaxies and DRGs with $K < 21$ (in Vega, ≈ 22.8 in AB) at $2 < z < 3.5$, respectively. According to Behroozi, Wechsler, & Conroy (2013), the mean stellar to halo mass ratio peaks at $M_H \sim 10^{12} M_\odot$ where M_*/M_H is ~ 0.02 and M_* is $\sim 2 \times 10^{10} M_\odot$. When the mass of a halo increases from $M_H = 10^{12}$ to $10^{13} M_\odot$, the stellar mass inside increases by only three times. Thus there is no wonder that halo masses of galaxies with stellar masses $M_* = 10^{10.5} - 10^{11} M_\odot$ range widely. Both the size and circular velocity of a halo are proportional to a cubic root of the halo mass, approximated with the spherical collapse model (Eq. (2) of Mo, Mao, & White 1998). Thus DRGs would have the disc sizes (and rotational velocities) twice larger than those of normal SFGs, consistent with the observed size difference of massive SFGs in the AzTEC14 group.

The sizes and stellar masses of massive SFGs in the AzTEC14 group are comparable to those of massive ETGs in the local Universe (Fig. 5). It is interesting to find a post starburst galaxy, Az14-K15a, composed of an AGN component and flat stellar component. The size and stellar mass growths via mergers can be less important for them to evolve into local massive ETGs. Even though they have late-type morphologies at this point, they can evolve into fast-rotating ETGs by exhausting gas (e.g., Khochfar et al. 2011). On the other hand, remarkable compactness of Az14-K15c implies the two-phase formation scenario in which massive compact ellipticals are formed at once and evolve into local massive ETGs through many mergers in later (Oser et al. 2010). Gas rich major mergers (Cox et al. 2006; Naab et al. 2007; Wuyts et al. 2010; Bournaud et al. 2011), and inflowing gas and wet mergers of inflowing clumps via disc instabilities (Dekel, Sari, & Ceverino 2009; Ceverino et al. 2015) can form massive compact ellipticals from large discy SFGs. Further studies of the relation between morphologies, stellar populations and also AGN activities in protoclusters, including such large and red SFGs, are needed to understand how massive SFGs transformed into massive ETGs today.

4.5 Stellar mass function and deficiency of low mass galaxies: The AzTEC14 group is a more massive group?

Given that many galaxies in the AzTEC14 group have sizes $r_e > 2$ kpc, source morphology is likely to affect severely on the detection completeness on not only our IRCS-AO K' -band but also MOIRCS K_s -band images. This suggests that stellar mass function obtained with MOIRCS in previous study is less complete than that we expected; stellar mass completeness limit can be twice larger ($\sim 10^{11} M_\odot$) and total flux values can be underestimated to reduce stellar masses estimates. Then the AzTEC14 group can be a group richer than that we claimed in previous study. Unfortunately, there may be no such a massive group in current large volume cosmological numerical simulations, since comparison groups of AzTEC14 group found in previous study is the richest groups in the Millennium simulation. Note that Hatch et al. (2009) reported that stellar mass function around the QSO at the center of a protocluster at $z = 2.16$, also a plausible progenitor of a BCG, is consistent with the galaxy formation models based on the Millennium simulation at $M_* > 10^{10} M_\odot$. But their results may be less affected by morphologies of galaxies since their targets are at the redshift lower than our target, i.e., less affected by cosmological surface brightness dimming, and they used the *HST* with the Strehl ratio higher than that of the AO188 in typical.

Much more deep imaging observations are required to measure stellar mass function robustly and show whether the observed deficiency of faint galaxies is originated in diffuse morphologies and/or actual deficiency of them. Suppressions of formations of low-mass galaxies by reionization (Bullock, Kravtsov, & Weinberg 2000) and supernovae feedbacks (Benson et al. 2002, 2003) are predicted but the strength of such effects are still open question. The large stellar mass existing in the group implies that it had the star formation density higher than that in general fields at past, i.e., there is a strong UV radiation field heating the gas of low mass halos. But the characteristic halo mass at which a halo lost half of its baryon by the reionization or supernovae feedback is too low ($M_H \sim 10^9 M_\odot$) to cause the deficiency of faint galaxies observed in the AzTEC14 group. On the other hand, supernovae feedbacks can work effectively to transport angular momenta from inner to outer-radii of galaxies to extend their sizes (Benson et al. 2002). It can also happen that gravitational heating prevents the cooling of low mass sub-halos since the AzTEC14 group can be (partly) virialized as it has the halo mass $M_H \sim 10^{13} M_\odot$ (Kubo et al. 2016).

5 CONCLUSION

We conducted the deep and high resolution imaging of an extremely dense group of galaxies, called the AzTEC14 group, at the core of the protocluster at $z = 3.09$ in the SSA22 field by using the AO188/IRCS equipped on Subaru Telescope to study morphological evolution of massive ETGs. Wide morphological variety of them implies that morphology-density relation today has just begun forming.

We confirm that one of the two QGs in the group, the most massive member, is a compact QG. This supports the

two-phase formation scenario of giant elliptical galaxies that massive compact ellipticals formed at once and they evolve in sizes and stellar masses by series of mergers. To form a local BCG-like object by $z \sim 1$, sometimes observed, in situ star formation in the group members may be important. Another QG in the group is fitted with the model composed of a nuclear component and not so compact Sérsic model, and shows double peaked and spatially extended [OIII] λ 5007 emission lines (~ 8 kpc). It is a key result to find an evidence of outflows from an AGN(s) in a young QG. Massive SFGs in the group have stellar masses and sizes comparable to those of local massive ETGs. Even if massive SFGs become compact spheroids at once by gas rich major mergers, large stellar masses of them imply the importance of star formations before violent morphological evolutions. Although we obtained the image more sensitive for typical $z \sim 3$ galaxies in general fields than our previous MOIRCS K_s -band image, no candidate new group members are detected. It implies that there is an actual deficiency of low mass galaxies and/or they are too diffuse to be detected on our IRCS-AO K' -band image. Moreover, given the morphological trend of the AzTEC14 group found in this study, our previous estimate of stellar mass function of the AzTEC14 group with MOIRCS is likely to be less complete than that we expected.

We argue the necessity of more careful treatments of diffuse and red galaxies at $z > 3$ which are hardly detected with the *HST* but may play important roles in massive galaxy formation. More deep and wide imaging surveys at wavelength longer than $2 \mu\text{m}$ with large telescopes are needed to study such red, diffuse and faint galaxies. Careful subtractions of AGNs from compact QGs and SFGs are also important to evaluate the size evolution history of massive ETGs correctly.

ACKNOWLEDGMENTS

This study is based on data collected at Subaru Telescope, which is operated by the National Astronomical Observatory of Japan. We would like to thank the Subaru Telescope staff for many help and support for the observations. Our studies owe a lot deal to the archival Subaru Suprime-Cam (Matsuda et al. 2004), *Spitzer* IRAC & MIPS data taken in Webb et al. (2009), *Chandra* data taken in Lehmer et al. (2009). We also thank to AzTEC/ASTE observers of the SSA22 field providing the updated source catalog. This work was supported by Global COE Program "Weaving Science Web beyond Particle-Matter Hierarchy", MEXT, Japan. YM acknowledges support from JSPS KAKENHI Grant Number 20647268. This work was partially supported by JSPS Grants-in-Aid for Scientific Research No.26400217. HU is supported by the ALMA Japan Research Grant of NAOJ Chile Observatory, NAOJ-ALMA-0071, 0131, 140, and 0152. HU is supported by JSPS Grant-in-Aid for Research Activity Startup (16H06713). This paper makes use of the following ALMA data: ADS/JAO.ALMA#2013.1.00162.S. ALMA is a partnership of ESO (representing its member states), NSF (USA) and NINS (Japan), together with NRC (Canada) and NSC and ASIAA (Taiwan) and KASI (Republic of Korea), in cooperation with the Republic of Chile. The Joint ALMA Observatory is operated by ESO, AUI/NRAO and NAOJ.

REFERENCES

- Andreon S., Dong H., Raichoor A., 2016, *A&A*, 593, A2
- Barnes J. E., 1989, *Natur*, 338, 123
- Behroozi P. S., Wechsler R. H., Conroy C., 2013, *ApJ*, 770, 57
- Benson A. J., Bower R. G., Frenk C. S., Lacey C. G., Baugh C. M., Cole S., 2003, *ApJ*, 599, 38
- Benson A. J., Frenk C. S., Lacey C. G., Baugh C. M., Cole S., 2002, *MNRAS*, 333, 177
- Benson A. J., Lacey C. G., Baugh C. M., Cole S., Frenk C. S., 2002, *MNRAS*, 333, 156
- Bernardi M., 2009, *MNRAS*, 395, 1491
- Bernardi M., Hyde J. B., Sheth R. K., Miller C. J., Nichol R. C., 2007, *AJ*, 133, 1741
- Bertin E., Arnouts S., 1996, *A&AS*, 117, 393
- Bett P., Eke V., Frenk C. S., Jenkins A., Helly J., Navarro J., 2007, *MNRAS*, 376, 215
- Bezanson R., van Dokkum P. G., Tal T., Marchesini D., Kriek M., Franx M., Coppi P., 2009, *ApJ*, 697, 1290
- Biggs A. D., Ivison R. J., 2008, *MNRAS*, 385, 893
- Bode P. W., Cohn H. N., Lugger P. M., 1993, *ApJ*, 416, 17
- Bournaud F., et al., 2011, *ApJ*, 730, 4
- Brammer G. B., et al., 2012, *ApJS*, 200, 13
- Brammer G. B., van Dokkum P. G., Illingworth G. D., Bouwens R. J., Labbé I., Franx M., Momcheva I., Oesch P. A., 2013, *ApJ*, 765, L2
- Bruzual G., Charlot S., 2003, *MNRAS*, 344, 1000
- Bullock J. S., Kravtsov A. V., Weinberg D. H., 2000, *ApJ*, 539, 517
- Burke C., Collins C. A., 2013, *MNRAS*, 434, 2856
- Ceverino D., Dekel A., Tweed D., Primack J., 2015, *MNRAS*, 447, 3291
- Chabrier G., 2003, *PASP*, 115, 763
- Collins C. A., et al., 2009, *Natur*, 458, 603
- Contini E., De Lucia G., Hatch N., Borgani S., Kang X., 2016, *MNRAS*, 456, 1924
- Cooper M. C., et al., 2012, *MNRAS*, 419, 3018
- Cox T. J., Dutta S. N., Di Matteo T., Hernquist L., Hopkins P. F., Robertson B., Springel V., 2006, *ApJ*, 650, 791
- Daddi E., et al., 2005, *ApJ*, 626, 680
- Damjanov I., et al., 2009, *ApJ*, 695, 101
- De Lucia G., Blaizot J., 2007, *MNRAS*, 375, 2
- Dekel A., Sari R., Ceverino D., 2009, *ApJ*, 703, 785
- Dressler A., 1980, *ApJ*, 236, 351
- Elmegreen B. G., Elmegreen D. M., 2006, *ApJ*, 650, 644
- Genzel R., et al., 2008, *ApJ*, 687, 59-77
- Genzel R., et al., 2006, *Natur*, 442, 786
- Grogin N. A., et al., 2011, *ApJS*, 197, 35
- Gunn J. E., Gott J. R., III, 1972, *ApJ*, 176, 1
- Guo Q., et al., 2011, *MNRAS*, 413, 101
- Harikane Y., Ouchi M., Yuma S., Rauch M., Nakajima K., Ono Y., 2014, *ApJ*, 794, 129
- Hatch N. A., Overzier R. A., Kurk J. D., Miley G. K., Röttgering H. J. A., Zirm A. W., 2009, *MNRAS*, 395, 114
- Hayano Y., et al., 2010, *SPIE*, 7736, 77360N
- Hayashino T., et al., 2004, *AJ*, 128, 2073
- Hine N. K., Geach J. E., Alexander D. M., Lehmer B. D., Chapman S. C., Matsuda Y., 2016, *MNRAS*, 455, 2363
- Ichikawa T., et al., 2007, *PASJ*, 59, 1081
- Ikarashi S., et al., 2015, *ApJ*, 810, 133
- Ilbert O., et al., 2013, *A&A*, 556, A55
- Khochfar S., et al., 2011, *MNRAS*, 417, 845
- Kobayashi N., et al., 2000, *SPIE*, 4008, 1056
- Kodama T., Tanaka I., Kajisawa M., Kurk J., Venemans B., De Breuck C., Vernet J., Lidman C., 2007, *MNRAS*, 377, 1717
- Koekemoer A. M., et al., 2011, *ApJS*, 197, 36
- Kubo M., et al., 2013, *ApJ*, 778, 170
- Kubo M., Yamada T., Ichikawa T., Kajisawa M., Matsuda Y., Tanaka I., Umehata H., 2016, *MNRAS*, 455, 3333
- Kubo M., Yamada T., Ichikawa T., Kajisawa M., Matsuda Y., Tanaka I., 2015, *ApJ*, 799, 38
- Laporte C. F. P., White S. D. M., Naab T., Gao L., 2013, *MNRAS*, 435, 901
- Larson R. B., Tinsley B. M., Caldwell C. N., 1980, *ApJ*, 237, 692
- Lehmer B. D., et al., 2009, *MNRAS*, 400, 299
- Lidman C., et al., 2013, *MNRAS*, 433, 825
- Lotz J. M., et al., 2013, *ApJ*, 773, 154
- Müller-Sánchez F., Comerford J. M., Nevin R., Barrows R. S., Cooper M. C., Greene J. E., 2015, *ApJ*, 813, 103
- Müller-Sánchez F., Prieto M. A., Hicks E. K. S., Vives-Arias H., Davies R. I., Malkan M., Tacconi L. J., Genzel R., 2011, *ApJ*, 739, 69
- Man A. W. S., et al., 2016, *ApJ*, 820, 11
- Marsan Z. C., Marchesini D., Bedregal A. G., Brammer G. B., Geier S., Labbe I., Muzzin A., Stefanon M., 2016, *arXiv*, arXiv:1606.05350
- Matsuda Y., et al., 2004, *AJ*, 128, 569
- Meza A., Navarro J. F., Steinmetz M., Eke V. R., 2003, *ApJ*, 590, 619
- Mo H. J., Mao S., White S. D. M., 1998, *MNRAS*, 295, 319
- Moody C. E., Romanowsky A. J., Cox T. J., Novak G. S., Primack J. R., 2014, *MNRAS*, 444, 1475
- Moore B., Katz N., Lake G., Dressler A., Oemler A., 1996, *Natur*, 379, 613
- Morishita T., Ichikawa T., 2016, *ApJ*, 816, 87
- Morishita T., Ichikawa T., Noguchi M., Akiyama M., Patel S. G., Kajisawa M., Obata T., 2015, *ApJ*, 805, 34
- Muzzin A., et al., 2013, *ApJ*, 777, 18
- Naab T., Johansson P. H., Ostriker J. P., 2009, *ApJ*, 699, L178
- Naab T., Johansson P. H., Ostriker J. P., Efstathiou G., 2007, *ApJ*, 658, 710
- Newman A. B., Ellis R. S., Andreon S., Treu T., Raichoor A., Trinchieri G., 2014, *ApJ*, 788, 51
- Olsen K. P., Rasmussen J., Toft S., Zirm A. W., 2013, *ApJ*, 764, 4
- Oser L., Ostriker J. P., Naab T., Johansson P. H., Burkert A., 2010, *ApJ*, 725, 2312
- Overzier R. A., et al., 2008, *ApJ*, 673, 143-162
- Papovich C., et al., 2012, *ApJ*, 750, 93
- Patel S. G., et al., 2013, *ApJ*, 778, 115
- Peng C. Y., Ho L. C., Impey C. D., Rix H.-W., 2010, *AJ*, 139, 2097
- Peng C. Y., Ho L. C., Impey C. D., Rix H.-W., 2002, *AJ*, 124, 266
- Peter A. H. G., Shapley A. E., Law D. R., Steidel C. C., Erb D. K., Reddy N. A., Pettini M., 2007, *ApJ*, 668, 23
- Quadri R., et al., 2007, *ApJ*, 654, 138
- Rujopakarn W., et al., 2016, *arXiv*, arXiv:1607.07710
- Sersic J. L., 1968, *adga.book*,
- Shankar F., et al., 2015, *ApJ*, 802, 73

Shibuya T., Ouchi M., Harikane Y., 2015, *ApJS*, 219, 15
 Shibuya T., Ouchi M., Kubo M., Harikane Y., 2016, *ApJ*, 821, 72
 Simpson J. M., et al., 2015, *ApJ*, 799, 81
 Springel V., et al., 2005, *Natur*, 435, 629
 Steidel C. C., Adelberger K. L., Dickinson M., Giavalisco M., Pettini M., Kellogg M., 1998, *ApJ*, 492, 428
 Steidel C. C., Adelberger K. L., Shapley A. E., Pettini M., Dickinson M., Giavalisco M., 2003, *ApJ*, 592, 728
 Stott J. P., Collins C. A., Burke C., Hamilton-Morris V., Smith G. P., 2011, *MNRAS*, 414, 445
 Stott J. P., et al., 2010, *ApJ*, 718, 23
 Tadaki K.-i., et al., 2014, *ApJ*, 788, L23
 Tadaki K.-i., Kodama T., Tanaka I., Hayashi M., Koyama Y., Shimakawa R., 2014, *ApJ*, 780, 77
 Tadaki K.-i., et al., 2015, *ApJ*, 811, L3
 Tamura Y., et al., 2009, *Natur*, 459, 61
 Toft S., et al., 2007, *ApJ*, 671, 285
 Trujillo I., et al., 2006, *MNRAS*, 373, L36
 Trujillo I., Conselice C. J., Bundy K., Cooper M. C., Eisenhardt P., Ellis R. S., 2007, *MNRAS*, 382, 109
 Trujillo I., et al., 2006, *ApJ*, 650, 18
 Uchimoto Y. K., et al., 2008, *ASPC*, 399, 373
 Uchimoto Y. K., et al., 2012, *ApJ*, 750, 116
 Uchimoto Y. K., et al., 2008, *PASJ*, 60, 683
 Umehata H., et al., 2014, *MNRAS*, 440, 3462
 Umehata H., et al., 2015, *ApJ*, 815, L8
 Umehata H., et al., 2017, *ApJ*, 835, 98
 van der Wel A., et al., 2014, *ApJ*, 788, 28
 van Dokkum P. G., et al., 2008, *ApJ*, 677, L5
 van Dokkum P. G., Kriek M., Franx M., 2009, *Natur*, 460, 717
 van Dokkum P. G., et al., 2010, *ApJ*, 709, 1018
 Vulcani B., et al., 2016, *ApJ*, 816, 86
 Wang T., et al., 2016, *ApJ*, 828, 56
 Williams R. J., Quadri R. F., Franx M., van Dokkum P., Labbé I., 2009, *ApJ*, 691, 1879
 Webb T. M. A., Yamada T., Huang J.-S., Ashby M. L. N., Matsuda Y., Egami E., Gonzalez M., Hayashimo T., 2009, *ApJ*, 692, 1561
 Welker C., Dubois Y., Devriendt J., Pichon C., Kaviraj S., Peirani S., 2015, *arXiv*, arXiv:1502.05053
 Wuyts S., Cox T. J., Hayward C. C., Franx M., Hernquist L., Hopkins P. F., Jonsson P., van Dokkum P. G., 2010, *ApJ*, 722, 1666
 Yamada T., Nakamura Y., Matsuda Y., Hayashino T., Yamauchi R., Morimoto N., Kousai K., Umemura M., 2012, *AJ*, 143, 79
 Yuma S., et al., 2013, *ApJ*, 779, 53
 Zhang Y., et al., 2016, *ApJ*, 816, 98
 Zhao D., Aragón-Salamanca A., Conselice C. J., 2015, *MNRAS*, 453, 4444
 Zirm A. W., et al., 2008, *ApJ*, 680, 224-231
 Zirm A. W., Toft S., Tanaka M., 2012, *ApJ*, 744, 181

APPENDIX A: INFLUENCE OF PSF VARIATION

In this work, we perform two-dimensional fits of galaxies adopting an observed image of the closest star to the image

center as a PSF reference. Since performance of an AO system is not uniform on the whole image, we need to concern influence of PSF variation on evaluating morphological properties. According to the performance of the AO188, FWHM of PSF sizes at our targets can be $-0''.02$ to $+0''.02$ different from that at the star adopted as a PSF reference in this study.

To test influence of PSF variation, we compare two-dimensional fits performed with different stars found in our image as PSF references. (R.A., Dec), FWHM PSF sizes, separations from TTGS and LGS of these stars are as follows; (22:17:37.644 +0:18:06.71), 0.16, 75 and 15 arcsec; (22:17:36.457 +0:18:34.00), 0.17, 44 and 18 arcsec; (22:17:35.648 +0:18:24.29), 0.18, 52 and 23 arcsec. Fig. A1 shows morphological properties evaluated by adopting different PSF references. Effective radii and Sérsic indices of galaxies measured with a star other than the PSF reference star adopted in this study are shown against those estimated by using the PSF reference star adopted in this study.

The influence of PSF variation on estimated effective radii is small except for a galaxy with the largest effective radius among the group. On the other hand, the estimates of Sérsic indices vary greatly by selections of PSF references.

APPENDIX B: REPRODUCIBILITY OF MORPHOLOGICAL PARAMETERS

Here we test reproducibility of morphological properties with the GALFIT. To test reproducibility of morphological properties, we generate mock galaxy images by making model galaxy images convolved with the observed PSF profiles by using the GALFIT and putting them on the blank fields of the observed image to add the sky fluctuation. Then we re-run the GALFIT.

We test the Sérsic models with the Sérsic indices ranging from $n = 0.5$ to 8, effective radii $r_e = 0.5$ to 8 kpc and total magnitudes $K_{tot} = 21.5 - 24.5$. We performed a thousand simulations for each model and see deviations of re-estimated values from inputs. Fig. B1 compares initial inputs and means of effective radii, Sérsic indices and total magnitudes measured on simulated images. Fig. B2 compares initial inputs and standard deviation of effective radii, Sérsic indices and total magnitudes measured on simulated images from their initial inputs.

Fitting errors get larger for models with fainter K_{tot} , larger r_e and n . For typical compact elliptical galaxies at $z \sim 3$ ($n \geq 2.5$ and $r_e = 0.5 \sim 1$ kpc) with $K_{tot} = 22$ ($K_{tot} = 22.5$), the 1σ rms errors of the re-estimated values from the model parameters are $\sigma_{r_e} = 0.3$ (0.5) kpc and $\sigma_n = 1$ (3). For typical late-type galaxies at $z \sim 3$ ($r_e = 0.5 \sim 2$ kpc and $n < 2.5$) with $K_{tot} = 22.5$ (24.0), the 1σ rms errors are $\sigma_{r_e} = 0.7$ (1.3) kpc and $\sigma_n = 0.4$ (1.9). For large late-type galaxies with $r_e = 3$ kpc and $K_{tot} = 22.5$ (24.0), the 1σ rms errors are $\sigma_{r_e} = 1.2$ (1.9) kpc and $\sigma_n = 0.4$ (2.8).

APPENDIX C: DETECTION COMPLETENESS

We test dependence of detection completeness on galaxy morphologies on both our IRCS-AO K' -band and MOIRCS K_s -band images by generating mock galaxy images by the

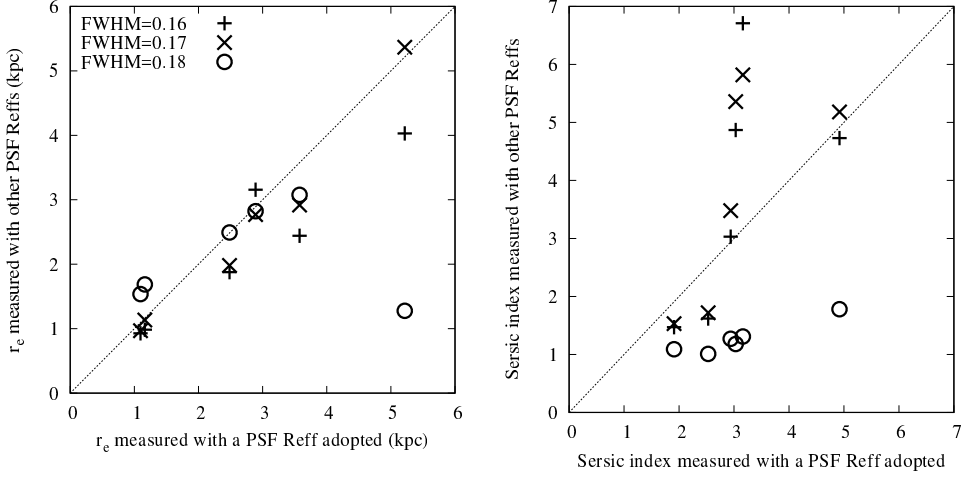


Figure A1. *Left:* Effective radii of galaxies estimated with the PSF reference star adopted in this study v.s. those estimated using other stars as PSF references. The crosses, x-marks and circles show in cases using stars with the FWHMs of the PSF sizes $0''.16$, $0''.17$ & $0''.18$, respectively, as PSF references. *Right:* Similar to the *left* panel but shows Sérsic indices n .

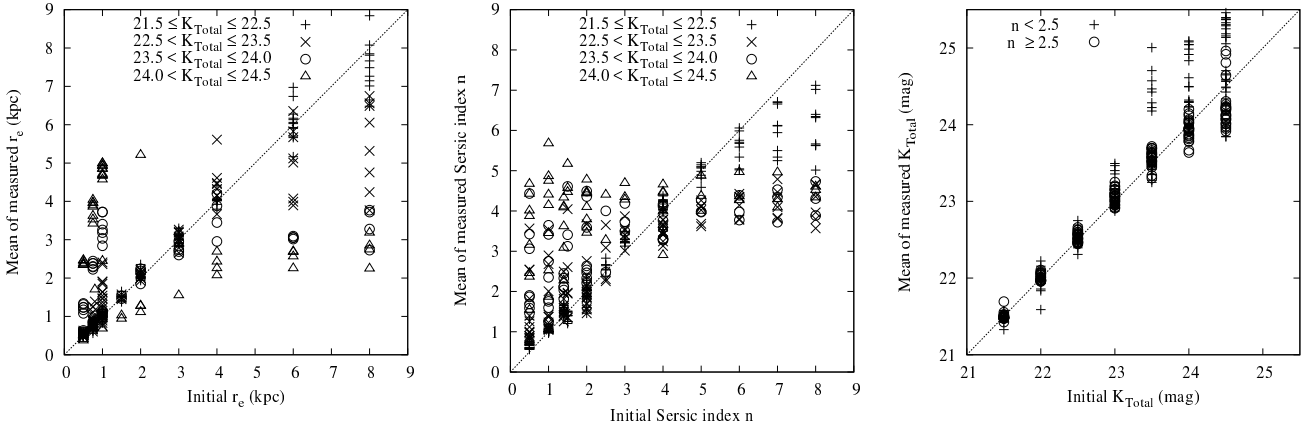


Figure B1. *Left:* Initial input effective radii v.s. means of effective radii measured on simulated images for models with $r_e = 1 - 8$ kpc, $n = 0 - 8$ and $21.5 \leq K_{\text{tot}} \leq 24.5$. The crosses, x-marks, circles and triangles show results for initial inputs of $21.5 \leq K_{\text{tot}} \leq 22.5$, $22.5 < K_{\text{tot}} \leq 23.5$, $23.5 < K_{\text{tot}} \leq 24.0$ and $24.0 < K_{\text{tot}} \leq 24.5$, respectively. *Center:* Similar to the *left* panel but for Sérsic indices. *Right:* Similar to the *left* panel but for total magnitudes. The crosses and circles show results for initial inputs of $n < 2.5$ and $n > 2.5$, respectively.

way described in Appendix B and extracting them by using the SExtractor (Bertin & Arnouts 1996). For MOIRCS K_s -band image, the PSF convolved with model galaxies is generated from stars observed simultaneously with our targets, where FoV of single MOIRCS detector is 3.5×4.0 , by PSF task of the IRAF. We extract sources detected over 1.5σ at each pixel ($1 \text{ pix} = 0''.052$ for IRCS and $0''.117$ for MOIRCS) for > 0.02 and $> 0.2 \text{ arcsec}^2$ adjacent areas on our IRCS-AO K' and MOIRCS K_s -band images, respectively.

Figure C1 and C2 show detection completeness in cases $n = 1$ & 4 and $r_e = 1 \sim 3$ kpc on our IRCS-AO K' -band and MOIRCS K_s -band images, respectively. Fig. C3 shows means of measured total magnitudes in cases $n = 1$ and $r_e = 1 \sim 3$ kpc on both IRCS-AO K' -band and MOIRCS K_s -band images.

Impact of object morphologies on detection completeness is stronger for models with low Sérsic indices on the

IRCS-AO K' -band image. In addition, detection completeness declines as sizes of objects increase. There are also significant underestimation of total magnitudes depending on sizes. Object morphologies is less strongly but also affect detection completeness on our MOIRCS K_s -band image. Objects with $K_{\text{tot}} < 24$ are almost completely detectable on our IRCS-AO K' -band image but their total fluxes are likely to be significantly underestimated.

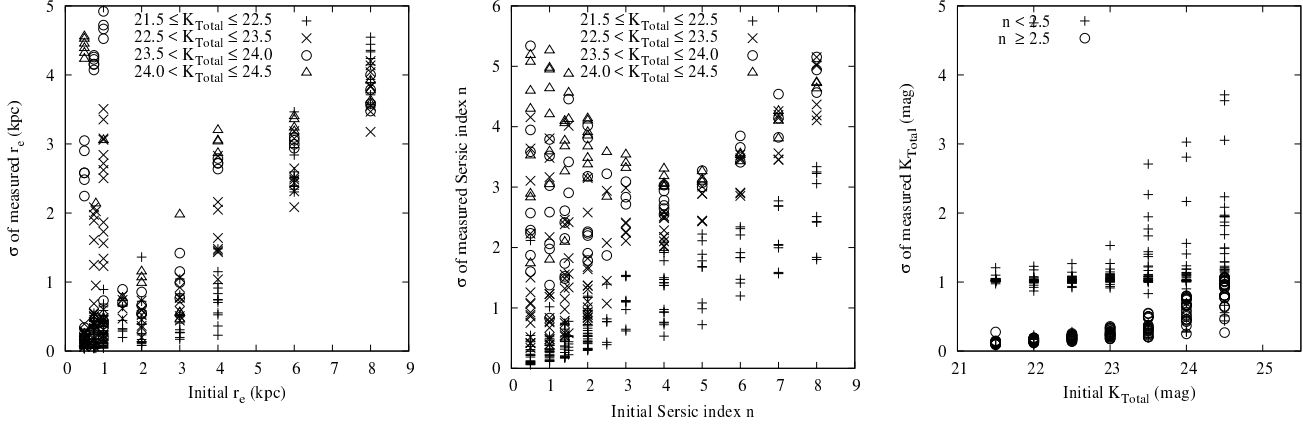


Figure B2. Similar to Fig. B1 but standard deviations of measured values from initial inputs are shown in y-axis.

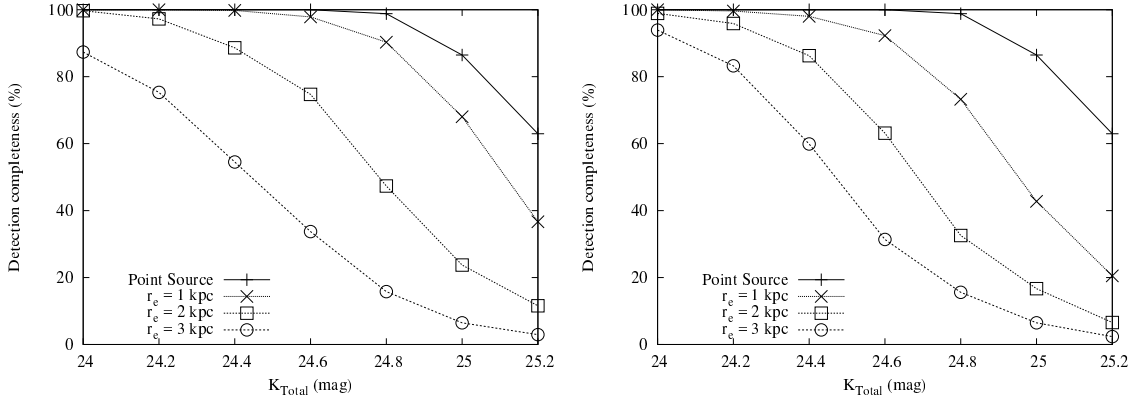


Figure C1. *Left:* Detection completenesses of models with Sérsic indices $n = 1$ on our IRCS-AO K' -band image. The x-marks, squares and circles with dot lines show detection completenesses of models with $r_e = 1, 2$ & 3 kpc, respectively. The cross-points with a solid line show that of point sources. *Right:* Similar to the *left* panel but for models with Sérsic indices $n = 4$.

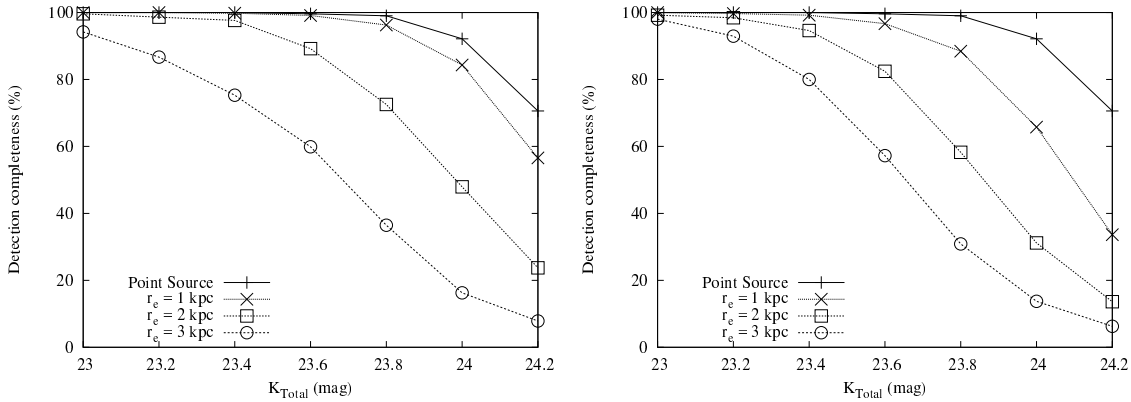


Figure C2. Similar to Fig. C1 but for our MOIRCS K_s -band image.

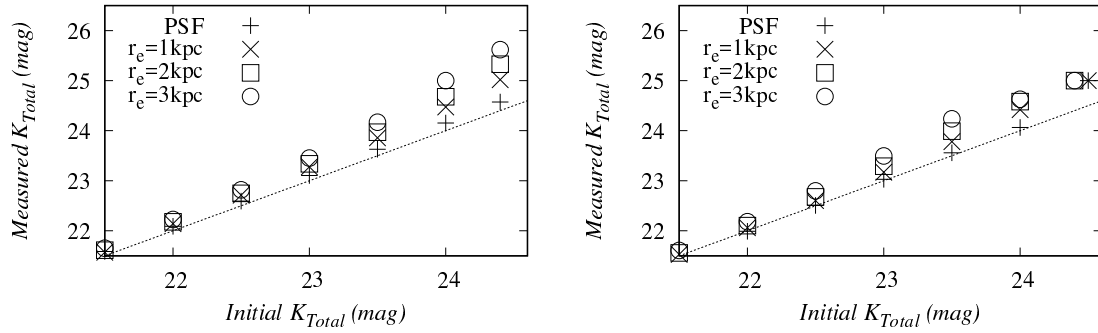


Figure C3. *Left:* Means of total magnitudes measured on simulated images of our IRCS-AO K' -band image for models with Sérsic indices $n = 1$. The x-marks, squares and circles show those of models with $r_e = 1, 2$ & 3 kpc, respectively. The cross-points show those of point sources. Means are taken for objects successfully detected on simulated images. The dot line shows the case that total magnitudes measured on simulated images properly reproduce initial input values. *Right:* Similar to the *left* panel but for our MOIRCS K_s -band image.